A Late Eocene- Oligocene through-flowing river between the Upper Yangtze and South China Sea

Peter D. Clift[1,2], Andrew Carter[3], Anna Wysocka[4], Hoang Van Long[5], Hongbo Zheng[2] and Nikki Neubeck[1]

1 - Department of Geology and Geophysics, Louisiana State University, Baton Rouge 70803, USA

2- Research Center for Earth System Science, Yunnan University, Kunming, Yunnan Province, 650091, PR China

3 - Department of Earth and Planetary Sciences, Birkbeck College, University of London, London WC1E 7HX, UK

4 - Faculty of Geology, University of Warsaw, Żwirki i Wigury 93, 02-089, Warsaw, Poland

5 - Vietnam Petroleum Institute, 167 Trung Kinh Distr. Yen Hoa Ward, Cau Giay District, Hanoi, Vietnam

Abstract

We test the hypothesis of a major Paleogene river draining the SE Tibetan Plateau and the central modern Yangtze Basin that then flowed South to the South China Sea. We test this model using

U-Pb dated detrital zircon grains preserved in Paleogene sedimentary rocks in northern Vietnam and SW China. We applied a series of statistical tests to compare the U-Pb age spectra of the rocks in order to highlight differences and similarities between them and with potential source bedrocks. Monte Carlo mixing models imply that erosion was dominantly derived from the Indochina and Songpan-Garzê Blocks and to a lesser extent the Yangtze Craton. Some of the zircon populations indicate local erosion and sedimentation, but others show close similarity both within northern Vietnam, as well as more widely in the Eocene Jianchuan, Paleocene-Oligocene Simao and Oligocene-Miocene Yuanjiang basins of China. The presence of younger (<200 Ma) zircons from the Qamdo Block of Tibet are less easily explicable in terms of recycling by erosion of older sedimentary rocks and imply a regional drainage linking SE Tibet and the South China Sea in the Late Eocene-Oligocene. Detrital zircons from offshore in the South China Sea showed initial local erosion, but with a connection to a river stretching to SE Tibet in the Late Oligocene. A change from regional to local sources in the Early Miocene in the Yuanjiang Basin indicates the timing of disruption of the old drainage driven by regional plateau uplift.

Keywords: Erosion, Indochina, Tibet, rivers, provenance, zircon

Introduction

The history of drainage evolution in SE Asia, SW China and the SE Tibetan Plateau has been a controversial topic for several years as a result of its importance in understanding the growth of topography in this region during the Cenozoic, most notably surface uplift of the Tibetan Plateau. The region is anomalous in terms of its drainage patterns because several large

47 rivers flow close together in SE Tibet, rather than showing a more typical dendritic pattern,
48 indicative of instabilities in the drainage evolution. Moreover, the Yangtze River, which starts on
49 the plateau and initially flows towards the southeast, experiences a reversal in flow direction
50 towards the northeast when it reaches the region of Yunnan in SW China (Fig. 1). Put together
51 these geometries are suggestive of a drainage system that has experienced major headwater
52 capture [*Brookfield*, 1998; *Clark et al.*, 2004]. The timing and nature of this capture should be
53 informative about the timing of uplift of the plateau because rivers must flow downhill. Also,
54 once flowing in deeply incised gorges, as they now do on the flanks of the plateau, capture of
55 drainage from one river by its neighbor is harder to achieve.
56 The single most important potential capture point is the First Bend in the Yangtze River
57 at Shigu (Fig. 1) where it has been hypothesized that the river used to flow further South and join
58 the upper reaches of what is now the Red River [*Clark et al.*, 2004]. The timing of formation of
59 the First Bend and the origin of the Yangtze River has been much debated, with a variety of ages
60 proposed spanning from the Eocene [*Richardson et al.*, 2010; *Zhang et al.*, 2014], to the early
61 Oligocene [*Chen et al.*, 2017; *Yan et al.*, 2012], to the Pleistocene [*Kong et al.*, 2009; *Kong et al.*,
62 2012]. In contrast some argue that no capture has ever taken place [*Wei et al.*, 2016]. Incision of
63 the river near the First Bend has variously been dated as Oligocene to Early Miocene [*Shen et*
64 *al.*, 2016] and between 18 and 9 Ma [*McPhillips et al.*, 2016] implying that the modern geometry
65 is at least that old. Nonetheless, a number of indicators now suggest that the Oligocene-Miocene
66 boundary, around 24 Ma, may be the time of major reorganization [*Clift et al.*, 2006a; *Zheng et*
67 *al.*, 2013]. This is largely supported by evidence indicating that a river very much like the
68 modern system was flowing into the lower reaches of the Yangtze basin before 23 but after 35
69 Ma [*Zheng et al.*, 2013]. Furthermore, bulk Nd isotopic analysis of sediment from the Hanoi

70 Basin indicates a major shift in compositions towards the modern values during the Oligocene
71 [*Clift et al.*, 2006a]. Detrital zircon U-Pb and Hf isotope data from upper Miocene sedimentary
72 rocks in the Red River Fault Zone in Vietnam has been used to argue that any connection to the
73 Yangtze River had been lost before their deposition [*Hoang et al.*, 2009]. The direction of Nd
74 isotopic change suggested loss of drainage from the Yangtze Craton, the ancient continental
75 block dominating central southern China, a shift that is consistent with Pb isotope data in detrital
76 feldspar grains [*Clift et al.*, 2008; *Zhang et al.*, 2014].
77 In this paper we focus on new evidence from a series of small pull-apart basins in NE
78 Vietnam, as well as the Yuanjiang Basin of SW China. The age of the Vietnamese basins used to
79 be considered as Miocene, or younger, but these have recently been reassessed and reassigned to
80 Eocene and early Oligocene depositional ages, making them much more significant for the
81 timing of drainage development. Earlier provenance analysis of sediments in the Vietnamese
82 region has been limited, although more work has been done in SW China where zircon U-Pb
83 ages have been used before to test the idea of drainage capture in this region. *Wissink et al*.
84 [2016] used statistical analysis to argue that much of the sediment deposited across the region
85 was similar and that observed mixed age spectra could readily be explained by erosion of local
86 basement sources. These workers compared samples from China and from the offshore Song
87 Hong-Yinggehai Basin (SHYB), originally dated by *Yan et al.* [2011], to argue against a
88 through-flowing major river since the Late Eocene, consistent with the original interpretation by
89 *Yan et al.* [2011] and with work South of the Yangtze First Bend [*Wei et al.*, 2016]. Nonetheless,
90 it should be noted that none of these studies had any Paleogene constraints in Vietnam and that
91 even in the SHYB, most of the dated samples were Neogene or Upper Oligocene. In contrast, *Lei*
92 *et al*. [2019] examined Oligocene sediments in the SHYB and adjacent Qiongdongnan Basin and

93 argued that starting in the Late Oligocene detrital zircons were deposited that are similar in their
94 age spectra to those from the Red River or coastal rivers of Vietnam, rather than having zircon
95 U-Pb ages indicative of a local origin, mostly Hainan.
96 In this study we use detrital zircon U-Pb dating to constrain the origin of the sediments in
97 the Vietnamese Paleogene basins and compare these data with those from younger deposits
98 preserved in basins along the Red River Fault Zone, as well as similar fluvial Paleogene
99 sedimentary rocks exposed in the Yuanjiang, Simao and Jianchuan basins of SW China, in the
100 South China Sea, and the modern river systems themselves. Our data only constrain the relative
101 flux of zircon grains from the various sources and are not easily extrapolated into a bulk
102 sediment budget for the evolving drainages. In order to do that a measure of relative zircon
103 fertility for the various sources would be needed and this does not yet exist. However, because
104 each tectonic block and drainage considered is generally large the average is more likely to lie
105 close to an upper continental crust average than would be the case for small catchments that
106 might be subject to major fertility issues because of lithologic heterogeneity. We examine the
107 evidence for there being a continuous major river system flowing from SE Tibet to the South
108 China Sea in the latest Eocene-Oligocene. This is practical because of the new data presented
109 and the development of more advanced statistical analytical methods that allow detrital age data
110 to be more objectively compared [*Saylor and Sundell*, 2016; *Sundell and Saylor*, 2017;
111 *Vermeesch et al.*, 2016].
112
113 **Geological Setting**
114 There are a series of modest sized pull-apart basins arranged along a larger tectonic
115 lineament that strikes NW-SE in northeastern Vietnam, sub-parallel to the main Red River Fault,

and which is known as the Cao Bang-Tien Yen Fault Zone (CBTYFZ) (Fig. 2). Only one study has attempted to constrain the motion of this fault [*Pubellier et al.*, 2003], and it is generally considered to be of similar age as the much better dated Red River-Ailao Shan Fault Zone (RRASFZ) [*Gilley et al.*, 2003; *Leloup et al.*, 2001; *Tapponnier et al.*, 1990], i.e., starting around 37 Ma and ceasing significant sinistral slip at ~15 Ma.

Paleogene Basins of Northern Vietnam

The structure of the basins is not well documented, although they appear to have suffered some transpression [*Pubellier et al.*, 2003], as well as the initial transtension and related subsidence. This later inversion is linked to the reversal of motion on the RRASFZ after ~5 Ma [*Rangin et al.*, 1995]. The strata are typically gently-dipping and cut by high-angle strike-slip faults, but are not strongly deformed [*Binh et al.*, 2003; *Fyhn et al.*, 2018]. The sediments in the NE Vietnamese basins are dominated by fluvial deposits, both proximal alluvial fans and cross-bedded, channelized sandstones. Some of the sequences contain lacustrine and flood plain facies, including the coal-bearing sequences at Na Duong (Fig. 2) [*Böhme et al.*, 2013; *Wysocka*, 2009]. In the Na Duong Basin coal-bearing lacustrine sediments contain large fossil trees, which are overlain by thick-bedded sandstones and minor coal interbeds. The coarsening-upward character indicates sedimentation by progradation of a river-fed delta into a freshwater lake or swamp, analogous to the Achafalaya swamp of the lower Mississippi River in the southern US. The point bars produced during the channel migration also demonstrate graded bedding in some places.

The NE Vietnamese basins were for a long time considered to be Miocene or younger in origin and fill [*Cuong et al.*, 2000], but their depositional ages have recently been revised. Studies of vertebrate fauna in the Cao Bang and Na Duong basins instead now indicate

sedimentation during the Late Eocene [*Böhme et al.*, 2013; *Böhme et al.*, 2011]. Mammal fossils from the Na Duong Basin also favor Late Eocene sedimentation [*Ducrocq et al.*, 2015]. However, new palynology assemblages indicate that the Cao Bang Basin dates from the early Oligocene [*Wysocka et al.*, 2018], and a similar age is likely applicable in the other basins of this region.

Paleogene Basins of SW China

We compare the sediments in the Vietnamese basins with equivalent deposits in SW China, namely the Simao, Yuanjiang and Jianchuan basins of Yunnan province (Figs. 1 and 3, 4). Like the Vietnamese basins these are pull-apart basins associated with major strike-slip fault activity during the extrusion of tectonic blocks in SE Tibet following India-Eurasia collision [*Morley*, 2002].

The Yuanjiang Basin is located immediately NE of the RRASFZ and its development is closely linked to the motion on that fault [*Schoenbohm et al.*, 2005]. This study recorded fine-grained lacustrine sediments at the base of the section that are overlain by fluvial sedimentary rocks, known as the Langdun Formation, which contain Late Oligocene and Miocene fossil plants [*Schoenbohm et al.*, 2005; *Schoenbohm et al.*, 2006]. The Langdun sedimentary rocks comprise proximal alluvial fan conglomerate units eroded from both limestones of the Yangtze Craton, as well as the Cenozoic RRASFZ gneisses, although more sandy, fluvial sedimentary rocks of the Transitional Sandstone are also exposed.

The Simao Basin is located west of the RRASFZ within the Qamdo Block (Fig. 1). The Cenozoic sedimentary rocks unconformably overlie a fill of Jurassic-Cretaceous rift sediment, and are deformed into a roughly N-S trending syncline. The lowermost Denghei Formation

contains ostracods that place a Paleocene-Upper Eocene age on the strata [*Zhang et al.*, 1996]. These are in turn unconformably overlain by the Mengla Formation, which is assigned an Upper Eocene-Oligocene age [*Liu et al.*, 1998; *Zhang et al.*, 1996]. The Denghei Formation is generally finer grained, being comprised of mudstones, siltstones and sandstones interpreted as the product of braided river sedimentation. The Mengla Formation is generally coarser, containing conglomerates but then fines up-section. The lowermost Mengla sedimentary rocks are interpreted as the product of sedimentation in an alluvial fan setting, transitioning into a braided river environment up-section. Both Simao Basin formations have previously been subject to detrital zircon U-Pb dating [*Chen et al.*, 2017].

Stratigraphy of the Jianchuan Basin

In the case of the Jianchuan Basin (Fig. 1), early mapping generally assigned much of the stratigraphy to Miocene and Pliocene depositional ages, although with some recognition that the oldest parts of the basin might be Paleogene [*Yunnan Bureau of Geology and Mineral Resources*, 1990]. Most recently the depositional ages in this area have also been revised as a result of radiometric dating of volcanic rocks and intrusions in the upper part of the sequence, which now limits sedimentation at the top of the section to being around 35 Ma, Late Eocene [*Gourbet et al.*, 2017]. The revised older depositional ages are consistent with the concept that these basins are pull-apart structures associated with strike slip faults trending towards the southeast out of the Tibetan Plateau. Radiometric ages show that the start of motion on the major structures was at ~35–37 Ma [*Gilley et al.*, 2003; *Leloup et al.*, 2001].

The stratigraphy within the Jianchuan Basin is quite complicated. The oldest sedimentary rocks, the Yunlong Formation, are generally fine-grained floodplain deposits and these are

185 overlaid by sandier units of the Baoxiangsi Formation, characterized by interbedded red
186 mudstones and fine sandstones, as well as proximal conglomerates [*Wei et al.*, 2016]. These
187 sandstones are overlain by thick-bedded pale sandstones of the Jinsichang Formation, with the
188 uppermost part of the sequence comprising coal-bearing mudstone and sandstones of the
189 Shuanghe Formation. It is these rocks which contain the Eocene igneous rocks that now revise
190 the age control [*Gourbet et al.*, 2017]. We consider the Jinsichang and Shuanghe Formations to
191 be lateral equivalents within a general fluvial floodplain environment, with the Jinsichang
192 Formation representing the alluvial channel and the Shuanghe Formation being the product of
193 sedimentation in a more lacustrine environment adjacent to the river. In this study we consider
194 samples taken from the Jinsichang, Baoxiangsi and Shuanghe Formations, all of which were
195 deposited in the Eocene.
196
197 **Sampling**
198 In addition to compiling pre-existing detrital U-Pb zircon data from the Jianchuan Basin
199 [*Wissink et al.*, 2016; *Yan et al.*, 2012](Fig. 4) we analyzed a new sample from the Shuanghe
200 Formation taken from a gravel quarry southwest of Jianchuan city (Sample 330-13), three
201 samples from the Baoxiangsi Formation (Samples JN-4, 5 and 10), and two samples of partly
202 volcaniclastic sediment, part of the Shuanghe Formation (Samples JN-18 and 19; Table 1; Fig.
203 4). Sample 330-13 is from sandstone interbedded with coals and underlying a laminated silty
204 lacustrine sequence. Locations of samples from the study of *Yan et al.* [2012] that are used in this
205 synthesis are also shown in Figure 4. Stratigraphic assignments are taken from *Yan et al*. [2012]
206 but with revised depositional ages. Other samples from the larger study of *Wissink et al.* [2016]
207 are also shown on Figure 4, but this study did not specify which formation each sample was

from, making them harder to correlate. The locations of some samples lie close to the boundaries between the Baoxiangsi and the Jinsichang Formations, but they can at least all be considered Eocene and fluvial. We attempt to assign these samples by overlaying their locations on the regional geological map of *Yunnan Bureau of Geology and Mineral Resources* [1990]. For simplicity we consider a sub-sample of the *Wissink et al.* [2016] analyses, sufficient to characterize the basin (i.e., Jian-11-08, Lim-12-42, Lim-12-26).

New samples were taken from sandstones in each of the NE Vietnamese basins, as well as the Jianchuan and Yuanjiang Basins, as shown on the maps (Fig. 1–4) with GPS locations provided in Table 1. Because the study involved single grain zircon dating, we preferentially targeted sandstones in each of these locations since the method generally restricts dating to grains >30 μm, because of the laser spot size. In Vietnam Samples CB4 and CB12 were taken from the upper, sandier division of the stratigraphy at Cao Bang, while the other CB samples were taken from the more conglomeratic lower division. At Lang Son Samples 330-1 and 330-2 were both taken from massive, well sorted, thick-bedded sandstone units (~15 m thick) interbedded with mudstones. At Na Duong samples were taken from adjacent beds within the sand and coal-bearing units of the Na Duong Formation in the middle of the stratigraphy exposed at the coal mine. The sandstones showed current-generated, cross lamination and large-scale (3–6 m) cross bedding indicative of sedimentation in a high energy channel environment.

Methodology

A suite of 29 major and select trace elements were measured on bulk samples from the Vietnamese samples using fused disc XRF technology at the GeoAnalytical Laboratory of Washington State University. Sandstones were powdered before being fused. Full analytical

details are provided by *Johnson et al*. [1999]. Analytical uncertainties for major elements are ~1% of the measured value, as determined from repeat analysis of a suite of nine USGS standard samples. Results are provided in Table 2.

Zircons were separated from the sandstones after crushing of the original samples and application of standard heavy liquid methods. This work was undertaken by GeoSep Services of Moscow, ID. After mounting U-Th-Pb isotopic compositions were determined at the London Geochronology Centre facilities at University College London using a New Wave 193 nm aperture-imaged, frequency-quintupled laser ablation system, coupled to an Agilent 7700 quadrupole-based ICP–MS. An energy density of ~2.5 J/cm^2 and a repetition rate of 10 Hz were used during laser operation. Laser spot diameter was 25 μm with a sampling depth of 5–10 μm. Sample-standard bracketing by measurement of external zircon standard PLESOVIC [*Sláma et al.*, 2008] and NIST 612 silicate glass [*Pearce et al.*, 1997] were used to correct for instrumental mass bias and depth-dependent intra-element fractionation of Pb, Th and U. Temora [*Black et al.*, 2003] and 91500 [*Wiedenbeck et al.*, 2004] samples were used as secondary zircon age standards. Over 100 grains were analyzed for each sample to provide a statistically robust dataset for lithologically diverse units [*Vermeesch*, 2004]. Age data were filtered using a ± 15% discordance cut-off. For grains with ages younger than 1000 Ma the $^{206}Pb/^{238}U$ ratio was used and the $^{207}Pb/^{206}Pb$ ratio was used for grains older than 1000 Ma. All measurements were processed using GLITTER 4.4 data reduction software [*Griffin*, 2008]. Time-resolved signals recording isotopic ratios with depth in each crystal enabled filtering to remove signatures owing to overgrowth boundaries, inclusions and/or fractures. Individual U-Pb ages are reported at 2σ, with data provided in the Geochron databank (https://www.geochron.org) and on the Mendeley database (doi:10.17632/k3bwtx74tg.1).

254 Kernel density estimations (KDE) provide robust age distributions and are presented in
255 the text for visual analysis of age population (n>3) distributions and abundance. Traditional
256 probability density functions may smooth older age populations that inherently have a greater
257 age error than younger populations at 1σ, therefore KDEs are favored in this study to prevent this
258 bias [*Vermeesch*, 2012].

259

260 **Results**

261 The petrology of the samples considered in this study was assessed through microscope
262 thin sections. Figure 5 shows some examples of the sediments dated. It is noteworthy that the
263 sediments are often poorly sorted, mostly ranging from silt to medium sand-sized. The matrixes
264 are typically muddy. The clastic grain mineralogy is dominated by quartz and plagioclase, with
265 lesser amounts of potassium feldspar and rock fragments. Cross-polarized examination
266 highlights the presence of muscovite, with relatively modest amounts of chromite, tourmaline,
267 rutile, and zircon being identified. The source terrains are clearly of continental bedrock type,
268 suggestive of the presence of granites and metamorphic rocks, but the mineral assemblages are
269 not distinctive of a particular area, given the diversity in the possible source terrains upstream.
270 Sedimentation appears to have been relatively high energy and is potentially proximal in several
271 examples although this does not rule out the role of flooding in major river channels, especially
272 based on the sedimentary structures observed at outcrop. In general, the sediments may be
273 described as being compositionally and texturally relatively immature.

274 The overall character of the sediment can be further assessed using the major element
275 geochemistry and select number of discrimination diagrams. Figure 6A shows the plot of *Singh*
276 *et al*. [2005] which was designed to highlight the influence of current sorting on bulk sediment

277 major element geochemistry. The composition of the new materials is compared with modern
278 river sediments from the modern Red and Yangtze River basins, as well as Cenozoic
279 sedimentary rocks from the Hanoi Basin. Sediment compositions range over a wide range but the
280 Vietnamese Paleogene rocks tend to plot towards the quartz end of the spectrum, suggesting that
281 clay, biotite and muscovite may have been preferentially removed due to current sorting,
282 assuming an approximate upper continental crustal (UCC) average composition for the starting
283 materials. In contrast, modern sediments in the Yangtze and Red rivers show greater enrichments
284 in phyllosilicates and clays than the Paleogene materials (Fig. 6A).

285 An alternative view of the nature of the bulk sediment composition is provided by Figure
286 6B. This discrimination diagram [*Fedo et al.*, 1995] shows how the Paleogene rocks in Vietnam
287 may have been affected by chemical weathering. This triangular plot allows us to calculate the
288 degree of weathering using the Chemical Index of Alteration (CIA) proxy [*Nesbitt et al.*, 1980].
289 Most of the samples considered in this work plot close to the illite end member and have CIA
290 values between 80 and 90, which indicates heavily weathered material. Fresh bedrock has a
291 value of around 50, while sediment that has completely broken down into clay byproducts has a
292 value of 100. The Paleogene rocks are also more weathered than rocks in the modern Red and
293 Yangtze rivers, as well as the older sedimentary rocks previously analyzed from the Hanoi Basin
294 [*Hoang et al.*, 2009]. This suggests that the environment of sedimentation was more prone to
295 chemical weathering than in the recent past. This may reflect either slower transport, providing
296 more time for chemical breakdown, particularly in floodplain environments [*Lupker et al.*, 2012]
297 and/or it may also reflect stronger chemical weathering as a result of a hotter or wetter
298 environment because warm, humid conditions are typically believed to drive faster rates of

299 chemical weathering [*West et al.*, 2005]. This means that if the sediments are proximal in their
300 depositional environment then the sources themselves may have been strongly weathered.
301 The first indication of source that can be derived from the zircon U-Pb analyses is
302 through consideration of the Th/U ratio, which has been commonly used to estimate origins
303 [*Maas et al.*, 1992]. Other studies suggest that Th/U values are largely reflections of protolith
304 characteristics and that discrimination of igneous from metamorphic zircons is best done with
305 cathodoluminesence images combined with Th/U values [*Harley et al.*, 2007; *Schulz et al.*,
306 2006]. According to the Th/U proxy however the great majority of the sediment grains appear to
307 be derived from igneous bedrocks rather than metamorphic rocks, with a significant minority of
308 transitional value and indeterminate origin (Fig. 7). This is true of all the major sediment groups
309 considered in this study, Neogene and Paleogene basins in Vietnam, Paleogene basins in SW
310 China, as well as the modern rivers. Of course, grains originally derived from igneous rocks may
311 also be recycled from sedimentary bedrock sources shortly before the time of deposition.
312 Nonetheless, the age spectrum of the zircon U-Pb crystallization ages may be used as a
313 discriminant of the origin. While individual peaks are rarely unique to a single source the
314 number, range and intensity of zircon U-Pb age peaks can be used to effect to constrain
315 provenance provided a sufficient number of grains has been measured. Figure 8A shows the
316 range of zircon ages analyzed in this work and compares them both with known thermal and
317 magmatic events in Asia, as well as existing ages from the Neogene pull-apart basins of
318 Vietnam, major regional rivers and select sediments from the Jianchuan Basin, Simao Basin and
319 Qiongdongnan Basin. A number of distinctive populations are seen in all sediments, especially
320 the Indosinian orogeny (~200–300 Ma), which is endemic across SE Asia [*Carter and Clift*,
321 2008; *Lepvrier et al.*, 2004]. None of the Vietnamese Paleogene sediments contain any Cenozoic

or Cretaceous zircon grains, although there is such a population in Sample MY4 from the Yuanjiang Basin. Most of the sediments also contain older populations. This is particularly true of Sample CB8 from the Cao Bang Basin that has a wide range of older zircons. In contrast, Sample TK2 from That Ke Basin is almost completely dominated by Triassic Indosinian (200–300 Ma) grains. Sediments from the Lang Son and Na Duong basins have significant populations of "Caledonian" zircons (400–550 Ma), which are seen less commonly at That Ke and Cao Bang. Older 1800–2000 Ma grains are common in the Baoxiangsi Formation samples from Jianchuan Basin, while 750–1000 Ma grains are common in the Shuanghe Formation samples (JN18 and JN19).

Discussion

We now attempt to constrain the source of the sediments in the Paleogene basins in Vietnam and SW China through comparison with sources upstream, as well as other sediments from the Cenozoic of this area. At first inspection Samples MY1, MY2, and MY3 from the Yuanjiang Basin appear quite similar to Samples TK1, TK2, and CB4, CB10 and CB12 from northern Vietnam, as well as some samples from the Jianchuan Basin (i.e., Shuanghe, Lim-12-42, Jinsichang, Lim-12-26). Figure 8A shows that the Vietnamese Paleogene detrital zircon ages differ from their Miocene equivalents preserved along the RRASFZ in the Yen Bai, Lao Cai and Song Lo basins (Fig. 1). These younger sediments contain Cenozoic zircons, as well as moderate amounts of Cretaceous and Neoproterozoic material that are less common in the older sediments. The youngest zircons were derived by erosion from the exhuming metamorphic rocks along the RRASFZ [*Clift et al.*, 2006b]. The Neoproterozoic grains would originally have come from the Yangtze Craton, but since that direct drainage connection no longer exists they could have been

recycled from sedimentary rocks, likely Triassic sandstones deposited in the aftermath of the Indosinian Orogeny, although some may also be eroded from the local basement exposed along the RRASFZ. Alternatively, the zircons were sourced directly from the Yangtze Craton prior to drainage capture. This highlights a common problem in this and other provenance studies of zircons being recycled from older sediments rather than directly from the bedrock source. Indeed, the siliciclastic sedimentary rocks of the Songpan-Garzê are themselves eroded from both North China and Yangtze Cratonic sources [*Weislogel et al.*, 2010; *Weislogel et al.*, 2006], resulting in non-unique age signatures. Recognizing whether grains are directly supplied or recycled is often hard or impossible and often relies on context. For example, zircons with a Qamdo Block signature in the modern Red River must be recycled from older sedimentary rocks because the modern river does not now drain this block.

In itself the contrast between Neogene and Paleogene is significant and indicates a change in sources between those times, although this is mostly in terms of the appearance of Cenozoic zircons in the Neogene sediments compared to the Paleogene. The Vietnamese Paleogene sedimentary rocks have similarities with some of their approximately synchronous neighbors in SW China. The Simao Basin differs the most from the Vietnamese basins in that the sediments in the Simao Basin contain many grains dating >750 Ma, while these are less common in Vietnam. With the exception of Sample MY-4, the Yuanjiang Basin samples compare closely with those from Vietnam in having a strong Indosinian (Triassic: ~200–300 Ma) population and a less abundant tail of older material.

Sediments from the Jianchuan Basin share many of the age peaks seen in Vietnam, although the Jianchuan samples have a more abundant population of 1800–2000 Ma zircons (Fig. 8A). There are some significant differences between the different studies which might be related

368 to different interpretations of the stratigraphy. Most notably the *Yan et al.* [2012] analysis from
369 the Shuanghe Formation is quite different from those of the *Wissink et al*. [2016] study, or the
370 new analysis in this work (Fig. 8A). The *Yan et al.* [2012] age spectrum is dominated by 200–
371 300 Ma grains but *Wissink et al*. [2016] identified significant numbers of both Cenozoic and
372 1800–1950 Ma grains, similar to the sample measured in this study. Both earlier analyses from
373 the Jinsichang Formation are dominated by a simple Indosinian population comparable to that
374 seen at That Ke and like the *Yan et al.* [2012] analysis of the Shuanghe Formation. The
375 Jinsichang samples are also like Samples MY1 and MY2 from the Yuanjiang Basin, as well as
376 Sample XGJ2400 from the Simao Basin. More source diversity is seen in the Baoxiangsi
377 Formation, although again the sample from *Yan et al*. [2012] differs in having a much larger
378 1800–1950 Ma population compared to the *Wissink et al*. [2016] analysis, but similar to new data
379 provided here. These Baoxiangsi Formation samples have significant similarities in their age
380 spectra compared to those from the Lang Son and Na Duong basins, as well as Sample MY3
381 from the Yuanjiang Basin. These sediments are dominated by Indosinian and Caledonian
382 populations, as well as a small number of zircons dating at 750–950 Ma. The older, Lower
383 Oligocene sample from the offshore Qiongdongnan Basin (Y211LO), shows a simple dominance
384 of Indosinian zircons, while the younger, Upper Oligocene sample (Y211UO) has greater
385 diversity, with significant numbers of older grains in addition to this prominent peak. In this
386 respect it has similarities with the sedimentary rocks dated from the Cao Bang Basin.
387 We can also compare the Paleogene sediments from Vietnam to the modern river systems
388 as well as basement source terrains (Fig. 8B), recognizing that those samples with low number of
389 grains have a larger probability that at least one fraction has been missed. It is clear that the only
390 source that could provide large volumes of Cenozoic grains would be the Qamdo Block of

391 southern Tibet [*He et al.*, 2014]. Many of the modern rivers and basement terrains include
392 Triassic Indosinian zircons, although only the Indochina Block itself is heavily dominated by this
393 population. Few of the modern rivers or basement sources are very similar to any of the
394 sedimentary rocks, with the exception of the sediments from the That Ke and Cao Bang basins
395 and Samples XJG1210 and XJG2400 from the Simao Basin, which are all very similar to the
396 Indochina block, and also the Dadu River (Fig. 1). Nonetheless, a match to the Indochina Block
397 would be consistent with local sources. It is noteworthy that the Song Lo is unique in showing a
398 strong Caledonian (400–550 Ma) population, which is not recognized as dominating any of the
399 known source terrains. Based on its location we would expect the Song Lo to be deriving
400 sediment from the Western Yangtze block and/or Cathaysia, although neither of those has yet
401 been shown to contain basement rocks of that age. This likely represents incomplete
402 characterization of these basement sources.
403 We can use statistical analysis to look more carefully at the relationships between the
404 different samples and their possible sources. Initially we look at a two-dimensional multi-
405 dimensional scalar (MDS) diagram using the methodology of *Vermeesch et al*. [2016]. In this
406 approach the Kolmogorov–Smirnov (K-S) test is used to compare the age spectra of each sample
407 to determine if they have similarities to their neighbors or not. Those with similar age spectra
408 plot close together on the diagram, while contrasting samples are widely separated. Figure 9A
409 shows the array of old and modern sediment samples considered in the study. The associated
410 Shepherd Plot (Fig. 9B), a scatterplot of the distances between points in the MDS plotted against
411 the observed dissimilarities shows a relatively good correlation, implying that the MDS plot is
412 meaningful. It is noteworthy that the zircons from the Vietnamese Paleogene sediments plot in
413 the center of the diagram, while the Neogene and several of the modern rivers plot to the right.

414 consistent with the KDE patterns indicating a real difference between their sources. The scatter
415 of compositions in the Paleogene is however significant. There is a strong clustering of values
416 close to compositions represented by the modern Yangtze at the First Bend (Shigu) as well as the
417 modern Song Da, largely eroding the Indochina Block (Fig. 1). Zircon populations from the Na
418 Duong Basin are close to those from the Cao Bang Basin and Sample MY1 from the Yuanjiang
419 Basin, as well as the new Shuanghe Formation sample from the Jianchuan Basin. Sediments
420 from That Khe are not far distant from the Shuanghe Formation measured by *Yan et al.*[2012], as
421 well as Samples MY2 and MY3 from the Yuanjiang Basin. Sample MY4 from Yuanjiang Basin
422 and Samples JN18 and JN19, volcaniclastic sediments from the Shuanghe Formation of the
423 Jianchuan Basin, as well as Sample CB8 from Cao Bang Basin bear no resemblance to any other
424 sediment and are likely dominated by local sources.

425 As inferred from the KDE diagrams we note that the Song Lo has little similarity to any
426 other zircon population. The Yalong River that drains the eastern flank of the plateau is also an
427 outlier, suggesting that the source regions of this river were not major contributors to the
428 sediments downstream. However, with just 80 grains from the Song Lo (80 grains = 29% chance
429 of missing a 5% fraction) and 98 from the Yalong (98 grains = 13%) these data are insufficient to
430 define new bedrock end members with at least a 95% statistical confidence of identifying a 5%
431 fraction contribution.

432 The Lower Oligocene sample (Y211LO) from the Qiongdongnan Basin is also unusual in
433 terms of its age spectrum and suggests a completely unique, local source. The Upper Oligocene
434 sample (Y211UO) has similarities both to the Baoxiangsi Formation from the Jianchuan Basin,
435 the Simao Basin of China, as well as to the Cao Bang and Na Duong basin sediments measured
436 by this study. Indeed, the association of the Baoxiangsi and Shuanghe-18 samples with the

Simao Basin and the Paleogene of Vietnam raises the possibility that these sediments share similar sources, consistent with the concept a major through-going river system.

Further detail can be revealed through the use of a three-dimensional MDS following the statistical methods of *Saylor et al*. [2018]. This method allows greater complexity to be understood, which is useful in a sedimentary system as diverse as this. We choose to plot the MDS diagram based on results derived from the K-S test (Fig. 10). In this plot we also include data from the basement bedrocks of the potential source regions, but not the modern rivers because of low numbers of grain ages for each that preclude a statistically robust comparison. Because the quality of the analysis is critically dependent on having a significant number of grains [*Pullen et al.*, 2014; *Vermeesch*, 2004], more than we have available from single samples, we pool samples together from the different basins and formations to increase the total number of grains for each depositional area and time in order to improve the statistics. The two-dimensional MDS plot is used to exclude Samples JN18 and JN19 as being dominated by local sources and thus atypical of the Shuanghe Formation, as well as Sample MY4 from the Yuanjiang Basin, and Sample CB8 from the Cao Bang Basin for the same reason. Samples from the Simao Basin are divided into an older/Lower Paleocene-Eocene group and a younger/Upper Eocene-Oligocene group.

The Cathaysia and Qamdo blocks plot on the edge of the cluster suggesting that they are not dominant sediment producers to any of the basins considered. Many of the Chinese Paleogene sediments plot between the Songpan-Garzê, (North and West), Yangtze Craton and Indochina Block source end members. The divergence with the Vietnamese samples indicates an additional source influencing this region and this may the sources of the modern Song Lo which cannot be accurately assessed in the absence of more data from that area. Nonetheless, strong

similarities continue to be seen between the Yuanjiang Basin, the Shuanghe and Baoxingsi formations of the Jianchuan Basin and the Cao Bang and Na Duong basins, consistent with the concept of a continuous river supplying many of the sub-basins. The Upper Oligocene sediment in the Qiongdongnan Basin also plots in this region of the MDS diagram, despite being somewhat younger than the Baoxiangsi Formation or the sediments from the Cao Bang Basin. The Yuanjiang Basin samples show similarity with samples from the That Ke and Lang Son basins, as well as those from the Shuanghe Formation. Sediments from the Upper Miocene basins of the RRASFZ are markedly different from all the Paleogene sediments, but are most similar to the Indochina and Hainan basement sources.

A useful result of these MDS analyses is that it allows the potential end member sources to be identified, which can then used for unmixing of the sediment compositions to determine general trends in sediment derivation.

Source Unmixing

We attempt to derive a more objective estimate of the varying contributions from different source terrains to the sediments and rivers of SE Asia using a recently developed Monte Carlo based method [*Sundell and Saylor*, 2017]. In this approach a number of potential sources were identified from the MDS plots and our knowledge of the geology. 10,000 attempts are made to replicate a particular detrital age spectrum through varying the contributions from the various sources in order to match the observed zircon age spectrum, with the best 1% selected. Of course, this type of mixing can only be as good as the definition of the source areas. Furthermore, there is the added complexity that material that was originally derived from one basement block might have been eroded and transported to form the sedimentary cover of a

different block from where it is then reworked. Recycling material out of older sedimentary sequences complicates the sediment unmixing and is known to affect the modern rivers, e.g., Triassic sandstone are major sources of sediment to the Red River and contain grains originally derived from the Yangtze Craton [*Clift et al.*, 2006b]. There is no simple, definitive way to remove the recycling effect, but it might be expected to influence all our samples. We look for systematic major changes in zircon age populations to quantify changes in provenance with the understanding that even apparently unique peaks might be recycled through older sedimentary deposits. Only in the case of the <100 Ma grains associated with the Qamdo Block is a direct connection most likely because there are few Cretaceous sedimentary rocks in the area and the age of crystallization is only moderately older than the age of sedimentation, reducing the influence of recycling. Although the unmixing method appears to be quite quantitative, it does not take into account differences in zircon abundance within different source units, or influences of recycling and grain size due to hydrodynamic sorting and so it is best used in a general fashion to look at overall trends in the zircon age spectra.

In this study we use the DZmix software of *Sundell and Saylor* [2017] in order to analyze the new data we present here, as well as a selection of the earlier dated rocks that we compare with those deposits. We undertake the modeling using the probability density function of the grouped samples. The results of the mixing analysis are provided in Supplementary Table 1 and shown graphically in Figure 11, where the preferred contributions based on the best D value of the K-S test are displayed, as well as those based on the V factor of the Kuiper test. Results from the cross-correlation method are only provided in the Supplementary Table 1. We further show the cumulative U-Pb age distributions for each sediment group and the best 5% of forward models based on the K-S test in Figure 12 so that effectiveness of the models can be determined.

506 Where the measured spectra fall closely within the model range the erosional budget estimate
507 may be considered high quality. In the case of the Vietnamese basins (Neogene and Paleogene),
508 the end members used were the West Yangtze Craton, Cathaysia, the Qamdo Block, Indochina
509 and the Songpan-Garzê Block. We considered the West and North Yangtze blocks, Indochina,
510 Songpan-Garzê and Qamdo blocks for the Jianchuan, Simao and Yuanjiang basins. In the
511 offshore Qiongdongnan Basin we also accounted for the presence of Hainan, in addition to the
512 sources used for the Vietnamese basins.
513 While the Lower Oligocene of the Qiongdongnan Basin appears to be largely locally
514 derived from sources typical of Hainan, the Upper Oligocene (Y211UO) spectrum is more
515 complicated and suggestive of supply from much wider drainage basin including Cathaysia and
516 Indochina, but also with some supply from the Qamdo Block, Songpan-Garzê and the Yangtze
517 Craton (Fig. 11L), indicative of the influence of a major regional river extending to the SE
518 Tibetan Plateau. This mixing model is also one of the best constrained of any in this study (Fig.
519 12L). Figure 11J show the range of results from the Na Duong Basin, with greatest supply from
520 the Indochina and Songpan-Garzê blocks, a characteristic that it shares with the Lang Son Basin
521 (Fig. 11H), although this latter model is not a very good fit (Fig. 12I). The alternative Kuiper test
522 derived estimates indicate significant differences from the K-S based models, with a dominance
523 by Songpan-Garzê zircons rather than Indochina zircons at Lang Son. The poor fit of the
524 observations and models may imply the influence of a source not accounted for in this study,
525 and/or poor characterization of the sources that we do consider. Erosion from the Songpan-Garzê
526 could imply sedimentation from a river extending onto the Tibetan Plateau, although this
527 influence could also be reworked from Triassic sedimentary rocks. The That Ke Basin K-S
528 model is dominated by Indochina sources, together with some Yangtze Craton and minor Qamdo

Block material. There was much less flux from the Songpan-Garzê, although the Kuiper test model is more abundant in these grains. Again, it should be noted that the That Ke model is one of the less good of those presented here (Fig. 12H). Sediments deposited at Cao Bang are quite variable and also imply sediment supply from a host of sources, including the Qamdo Block and large amounts from the Yangtze Craton that might be recycled, although the large quantities involved are suggestive of a direct connection (Fig. 11G). The Cao Bang model is also one of the better from the northern Vietnamese basins (Fig. 12G), despite still being deficient in 1000–2000 Ma grains.

We note that the Miocene basins along the RRASFZ contain zircons of much different character to the Paleogene examples discussed above. The population is largely explicable simply in terms of erosion from the Indochina Block (~91%), although again the model fit is not good in the 1000–2000 Ma range (Fig. 12K). The Miocene sediments even contrast with the modern Red River at Lao Cai and Hanoi (Supplementary Table 1) where ~76% Indochina supply is estimated at each location, albeit recognizing that this number is based on low sample numbers. Theoretically the 4 and 10% Songpan-Garzê supply estimated at Hanoi and Lao Cai respectively should be impossible now that this terrain lies outside the modern drainage and this contribution must therefore reflect recycling from older sedimentary rock sources within the basin. Likewise, the low contribution from such a source during the Miocene does not imply a direct connection at that time. Presumably the rocks that are now suppling Songpan-Garzê-like zircons to the modern river were not being eroded in the Miocene, reflectin progressive uplift.

Sediments from the Upper Oligocene-Miocene Yuanjiang Basin show strong erosion from Indochina, similar to the That Ke and Lang Song basins (Fig. 11F). Nonetheless, there is still some influence from the Yangtze Craton, Songpan-Garzê and Qamdo blocks implying a

552 regional drainage. To the west, the older parts of the Simao Basin show strong erosion from the
553 local Indochina basement, but also supply from the Qamdo Block which is hard to explain in
554 terms of recycling from older sedimentary rocks (Fig. 11D). The younger Eocene-Oligocene
555 Simao Basin sediment is quite different and is explicable by erosional supply from the Indochina
556 and the Songpan-Garzê (Fig. 11F).
557 The mixing software makes somewhat different predictions for sediments from the
558 Jianchuan Basin, which is perhaps not surprising given their upstream location. The Jinsichang
559 Formation is unique in showing an almost total dominance of erosion from the Indochina Block.
560 This is the local basement and might imply little sediment derivation from SE Tibetan Plateau.
561 This conclusion is however not entirely clear because of ongoing debate regarding tectonic
562 affinity of crustal blocks in southern Tibet. While *Metcalfe* [1996] correlates the Qiantang
563 Terrane (located south of the Qamdo Block *sensu stricto*) with the Sibamasu Block of SE Asia,
564 as shown in our Figure 1, other workers correlate the Qiantang Terrane with Indochina instead
565 [*Searle et al.*, 2017]. If that correlation is more appropriate, then Indochina-type zircon
566 assemblages could be carried from the north into the Jianchuan Basin area. This scenario might
567 be considered quite likely given unmixing estimates from the modern Yangtze at the First Bend
568 (Shigu) indicating ~60% of the zircon population to be explicable by erosion of Indochina,
569 which most tectonic maps of the region do not show exposed upstream of that point
570 (Supplementary Table 1). Zircon populations from the similar aged and well modelled Shuanghe
571 Formation (Fig. 11C and 12C) also point to most sediment being derived from Indochina sources
572 but with more influences from all the other terranes of SE Tibetan Plateau. The older Baoxiangsi
573 Formation shows the greatest diversity in the modelled sources contributions (Fig. 11B).
574 Indochina was still important but erosion from Songpan-Garzê, the Yangtze Craton and the

575 Qamdo Block is also noted. These results argue against solely local erosion and sedimentation,
576 and imply a drainage basin extending at least into the Songpan-Garzê and likely to southern
577 Tibet. The presence of Songpan-Garzê zircons, both in the Jianchuan and Vietnamese basins
578 would be consistent with sedimentation from a major through-flowing river.
579 The results of the un-mixing calculations show that there are some Paleogene sediments
580 in both China and Vietnam that could have been locally derived. Nonetheless, the modelling
581 show that there were sediments sourced from the flank of the Tibetan Plateau and transported to
582 SW China and northern Vietnam in the Eocene-Oligocene, and even into the South China Sea at
583 least by the Late Oligocene. Compositions were not steady state but did involve erosion from a
584 consistent set of end members and these patterns are seen across several basins. The influence of
585 sources such as the West Yangtze Craton, Songpan-Garzê and Qamdo Blocks quite far
586 downstream in many of the basins implies the presence of a major river that would have been
587 able to supply these over long distances. This situation was disrupted by the Late Miocene when
588 sands derived almost exclusively from Indochina sources were deposited in pull-apart basins
589 along the RRASFZ. Subsequent further uplift has caused older sedimentary rocks, likely
590 Triassic, to be incised and eroded into the modern river.
591
592 **Statistical Comparisons**
593 As an alternative approach to identifying similar sediments within the various basins of
594 the study we also employ the DZStats software of *Saylor and Sundell* [2016]. We used the
595 software to make K-S tests between the observed spectra of the different sediments, as well as
596 the source regions in order to highlight potential similarities. The results of this analysis are
597 shown graphically in Figure 13. What is apparent is that the sediments from northern Vietnam

598 are relatively similar to one another, with the important exception of the Cao Bang Basin being
599 different from the Lang Son Basin. The former shows fewer Indosinian grains and less erosion
600 from Indochina, but more zircons from the Qamdo Block and the Yangtze Craton. The
601 Paleogene Vietnamese basins are also quite similar to the Paleocene-Eocene sediments from the
602 Simao Basin, and to a lesser extent to the Eocene-Oligocene from that basin. Again, the Lang
603 Son Basin shows the least commonality with the Simao Basin, especially with the Eocene-
604 Oligocene sediments. Samples from the Oligocene-Miocene Yuanjiang Basin show quite close
605 similarity with the Vietnamese basins, being especially close to the Na Duong Basin, despite the
606 difference in depositional age.

607 When we compare the analyses from the southern basins with the more northerly
608 Jianchuan Basin we note significant similarities, except with the Jinsichang Formation, which
609 appears to be a completely separate sediment system. In contrast, the Baoxiangsi and Shuanghe
610 formation samples are similar to many of the Vietnamese Paleocene (Lang Son Basin being the
611 least good match), as well as with the Simao Basin, especially the Paleocene-Eocene samples. A
612 roughly similar sediment source is implied despite the significant lateral distances involved and
613 the contrasting local basement compositions.

614 When we look further offshore into the Qiongdongnan Basin the Upper Oligocene
615 sample shows the closest similarities with sediments from the Simao Basin and with both
616 Shuanghe and Baoxiangsi sediments from the Jianchuan Basin, and to a slightly lesser extent
617 with the Yuanjiang Basin. The Qiongdongnan zircon spectrum is also similar to those measured
618 from the Cao Bang, That Ke and Na Duong basin sediments, but not with the Lang Son Basin.

619 When we compare the source spectra with the detrital measurements some general
620 patterns are noted. The West Yangtze Craton is similar to the Cao Bang Basin and Eocene-

621 Oligocene of the Simao Basin, as well as to the Upper Oligocene from Qiongdongnan Basin.
622 Indochina and the Songpan-Garzê show the most similarities to the Paleogene sedimentary rocks
623 across the entire area, except for the Jinsichang Formation of the Jianchuan Basin. The strong
624 Songpan-Garzê influence seen from the Jianchuan Basin to the Qiongdongnan Basin is unlikely
625 to simply be the sole result of recycling and likely represents a common source within that
626 terrain in the Eocene-Oligocene. The North Yangtze Craton, as well as Cathaysia, never
627 dominated any of the sediments. The Qamdo Block made modest contributions, but these are
628 commonly seen across the region and are hard to explain by recycling from older strata. Taken
629 together this implies a large regional river system flowing from SE Tibetan Plateau to the South
630 China Sea.

631 The statistical comparison is also useful in showing when this system came to an end.
632 The Upper Miocene sediments from the RRASFZ are quite different from the older sediments
633 regardless of location, implying a major change of regime. The age control from the Ailao Shan
634 Conglomerate of the Langdon Formation in the Yuanjiang Basin indicates that the older drainage
635 survived until the Late Oligocene-Miocene, but must have been lost soon after.

636 The development of the drainage can be understood in outline at least by considering how
637 the provenance and the tectonics have co-evolved in this area during the Cenozoic. We use the
638 simplified tectonic terrane model shown in Figure 1B and impose the strike-slip offsets along the
639 RRASFZ estimated by *Morley* [2002] to demonstrate how the basins have moved relative to the
640 source terrains through time. Although we recognize that other reconstructions indicate much
641 greater degrees of motion between Indochina and mainland Asia [*Replumaz and Tapponnier*,
642 2003] this matter continues to be controversial and is beyond the scope of this contribution. We
643 simplify the provenance using the estimates derived from the unmixing modelling described

644 above (Supplementary Table 1) as applied to four time slices: Late Eocene-early Oligocene,
645 Mid-Late Oligocene, Mid-Late Miocene and the present day (Fig. 14). Accounting for recycling
646 from older sedimentary rocks can be difficult, as shown by the modern river, which displays
647 significant short time and distance variability. The major differences between the Red River at
648 Lao Cai and Hanoi probably relate to instability in the sediment load driven by post-glacial
649 climate change [*Hoang et al.*, 2010] and possible anthropogenic disruption, as well as in
650 shortcomings in the models, especially that for the sample from the Red River at Lao Cai.
651 Nonetheless, the difference between the modern sediments and the Mid-Upper Miocene samples
652 is noteworthy. Clearly recycling allows Qamdo and Songpan-Garzê material to be eroded into
653 the modern river without a direct connection to these terrains. The lack of a similar signature in
654 the Miocene indicates that the modern signal comes from erosion of older sedimentary rocks that
655 were not yet uplifted and incised in the Miocene.
656 The Late Eocene-Early Oligocene map shows significant provenance variability across
657 the area, some of which may reflect temporal variability and evolution of the sediment load from
658 headwaters to the depocenter as the mainstream was joined by tributaries. Nonetheless, it is clear
659 that a Qamdo Block contribution is present throughout and that as noted above this is less
660 sensitive to recycling. This implies a connection by the paleo-Red River drainage to the SE
661 Tibetan Plateau at that time. The abundance of material from the Songpan-Garzê is also
662 suggestive of a link to that area, one that was broken by the Miocene. The Qiongdongnan Basin
663 sample from the Late Oligocene is especially powerful in requiring the presence of a major
664 drainage feeding into South China Sea at that time, originating in the Qamdo Block.
665 The results of this work have implications for the uplift history of the SE Tibetan Plateau.
666 The study confirms a large, pre-capture Red River stretching from the Qamdo and Songpan-

667 Garzê blocks to the South China Sea during the Late Oligocene (23–27.8 Ma), consistent with
668 the zircon data from the Yuanjiang Basin, whose depositional age is rather loosely constrained as
669 Upper Oligocene-Miocene (16–27.8 Ma) [*Schoenbohm et al.*, 2005; *Schoenbohm et al.*, 2006].
670 At the same time zircon data from the lower Yangtze River indicate that the head water capture
671 at the First Bend should have occurred prior to 23 Ma [*Zheng et al.*, 2013], and must have been
672 before accumulation of the Mid-Upper Miocene strata in the Yen Bai and Song Lo basins.
673 Because capture is most easily achieved in the earliest stages of surface uplift, before the rivers
674 are deeply entrenched in deep valleys, our preferred reconstruction favors major surface uplift in
675 the region of the Yangtze First Bend in the Late Oligocene, possibly starting in the Early
676 Oligocene. This is broadly consistent with the timing of the first initial uplift at 30–25 Ma
677 favored by *Wang et al.* [2012] in SE Tibet, and the outward growth model of W*ang et al*. [2014],
678 which advocated Paleogene uplift of the southern central plateau, but uplift around the edges
679 after 20 Ma. *Royden et al.* [2008] also suggested uplift of eastern Tibet starting after 20 Ma,
680 which is younger than would be inferred from this study. However, our results imply that the
681 model of *Hoke et al*. [2014] which called for a plateau as high as the modern in northern Yunnan
682 by the Late Eocene, and based on stable isotope data, may overestimate the degree of early
683 uplift.
684
685 **Conclusions**
686 In this study we U-Pb dated zircon crystals taken from a number of sands deposited
687 during the Eocene to Oligocene in northern Vietnam and SW China within a series of pull-apart
688 basins. Because the source areas upstream of these basins have resolvably different zircon U-Pb
689 age characteristics we attempt to define the dominant sources for the sediments and compare

690 them across the region, as well as downstream in the offshore Qiongdongnan Basin. It is clear
691 that the U-Pb age spectra of some of the sediments have little relationship to others and are
692 suggestive of erosion and sedimentation from local sources, as previously suggested [*Wissink et*
693 *al.*, 2016]. In general, the sediments however have complicated age spectra, indicative of erosion
694 from diverse source terrains, not all explicable by local sources and recycling. Paleogene
695 sedimentary rocks in Vietnam differ from Neogene rocks exposed close by, mostly by the
696 presence of Cenozoic and <200 Ma grains in the Paleogene sediment. This indicates a significant
697 change in the source of sediment from the Oligocene into the Late Miocene, by which time much
698 of the erosion was limited to the Indochina Block. Although a Lower Oligocene sample from the
699 Qiongdongnan Basin had a local Hainan source [*Lei et al.*, 2019], the Upper Oligocene sample
700 showed much greater diversity, consistent with a major river supplying material from the Qamdo
701 and Songpan-Garzê blocks into the deep water South China Sea by that time. Lack of Oligocene
702 or older sediments in the more proximal parts of the SHYB preclude demonstration of a
703 continuous link between northern Vietnam and south of Hainan during the Oligocene.
704 Most of the Paleogene sediments from northern Vietnam and SW China derive most of
705 their zircons from the Songpan-Garzê, Indochina and West Yangtze blocks, although much of
706 this material may be recycled through older sedimentary rocks, largely deposited in the aftermath
707 of the Triassic Indosinian Orogeny. We have to assume that zircon fertility differences between
708 the different source areas is not great and that the zircon budget resembles the bulk sediment
709 flux.
710 The presence of younger Qamdo Block derived zircons in the Paleogene sediments
711 cannot be explained by this process and argues for a major drainage originating in the SE Tibetan
712 Plateau. Many of the sediments in the Cao Bang, That Ke, Lang Son and Na Duong basins have

zircon U-Pb ages that are broadly consistent with erosion from similar sources. This overall similarity is consistent with deposition from a single coherent river system, albeit one that was experiencing moderate changes in composition through time. These sedimentary rocks also bear some similarities to rocks in the Simao, Yuanjiang and Jianchuan basins, most notably in the Eocene Baoxiangsi and Shuanghe Formations in the case of the Jianchuan Basin. Stratigraphic complexity/uncertainties however presently prevent us from making very precise correlations. Sediments from the Na Duong Basin appear to offer the closest match with the Yuanjiang Basin, while Na Duong and That Ke basins are closest to the Shuanghe Formation of the Jianchuan Basin. Paleocene-Eocene Simao Basin sediments have zircons with age spectra similar to both the Baoxiangsi and Shuanghe Formations of the Jianchuan Basin and those in northern Vietnam. Because the age control is not very precise it is possible that some of the provenance variability may be related to temporal evolution in the drainage basin. In any case we would not anticipate a perfect match between SW China and northern Vietnam because of the effects of local tributaries joining the mainstream between these areas which must necessarily result in an evolving composition. Nonetheless, the broad similarity of Paleogene sediments in these regions and the suggestion of original erosion in SE Tibet is consistent with the idea of there being a major through-going river system flowing from the SE Tibetan Plateau to the South China Sea during the Late Eocene-early Oligocene. The change seen up-section in the Yuanjiang Basin from regionally derived to local RRASFZ sources may indicate the end of the former drainage in the Early Miocene, likely because of headwater capture influenced by the motion on the RRASFZ.

Acknowledgements

735 PC is grateful for support from the Charles T. McCord Chair in Petroleum Geology at Louisiana
736 State University, as well as the Jackson School of Geosciences at the University of Texas at
737 Austin and the University of Hong Kong for the time to work on these topics. The work was
738 improved based on detailed comments from Joel Saylor, Andrew K. Laskowski and an
739 anonymous reviewer, as well as associate editor Peter van der Beek. This work was partly
740 supported by the Second Tibetan Plateau Scientific Expedition and Research (STEP)
741 (2019QZKK0704), the Strategic Priority Research Program of Chinese Academy of Sciences
742 (XDB26020301), NSFC（U1902208, 41991323) and Vietnam National Foundation for Science
743 and Technology Development (Nafosted - 105.01-2011.18). We thank Paul O'Sullivan and
744 colleagues at GeoSep for their help with mineral separation. New data produced by this project is
745 stored with the Mendeley repository (doi:10.17632/k3bwtx74tg.1) and the zircon U-Pb data also
746 with the Geochron databank (https://www.geochron.org).
747
748

749 **Figure Captions**

750

751 Figure 1. A) Shaded topographic map of East and SE Asia showing the major modern river
752 basins and the location of Well Y211 [*Lei et al.*, 2019], CP – Chao Phraya, SW – Salween. B)
753 Shaded topographic map of the study region showing the major river systems and geographic
754 regions mentioned in the text. CBTYF - Cao Bang-Tien Yen Fault Zone. International borders
755 shown as dashed black line. River names are show in yellow italic text. C) Simplified tectonic
756 map of the region showing the major tectonic blocks and the course of the major rivers discussed
757 in this work, modified from original map of *Searle et al. [2017]*.

758

759 Figure 2. A) Satellite image of northern Vietnam showing the setting of the four groups of
760 samples considered in this study. B) Geological map of northern Vietnam with the sampled
761 Cenozoic basin highlighted [*Fromaget et al.*, 1971].

762

763 Figure 3. A) Satellite photograph of the Yuanjiang Basin region close to Yuanjiang town.
764 Locations of samples (white dots) dated in this study are shown. B) Geological map of the
765 Yuanjiang Basin. Map modified from *Schoenbohm et al.* [2005].

766

767 Figure 4. A) Satellite photograph of the Jianchuan Basin and Yangtze First bend region close to
768 Shigu town. Locations of samples (white dots) discussed in this study are shown. Lim- and Jian-
769 samples are from *Wissink et al.* [2016], named samples are from *Yan et al*. [2012]. Sample 330-
770 13 is new. B) Geological map of the Jianchuan Basin relative to Shigu and the first bend. Map
771 modified from Y*unnan Bureau of Geology and Mineral Resources* [1990].

772

773 Figure 5. Photomicrographs of some of the samples considered in this study. A) Plane polarized
774 and B) cross polar image of Sample 330-1 from Lang Son. Poorly sorted sandstone dominated by
775 quartz, feldspars and rock fragments with a muddy matric and minor limonite. C) Sample 330-2
776 also from Lang Son. Quartz and rock fragment dominated sandstone with muddy matric and
777 large flakes of muscovite. D) Sample 330-3 from the Na Duong coal mine characterized by
778 poorly sorted quartz and rock fragments with minor chromite, tourmaline, rutile and zircon.
779

780 Figure 6. A) Al_2O_3/SiO_2 versus Fe_2O_3/SiO_2 for river sediments analyzed by this study.
781 Lower/higher ratios indicate increase of the quartz proportion and enrichment of phyllosilicates,
782 respectively [*Singh et al.*, 2005]. Linear trend corresponds to mineralogical sorting of these
783 sediments during fluvial transportation. Star corresponds to average upper continental crust
784 (UCC)[*Taylor and McLennan*, 1995]. Modern Vietnamese river and Hanoi Basin data are from
785 *Clift et al.* [2008]. Upper Yangtze data are from *He et al.* [2014]. B) Geochemical signature of
786 the analyzed samples illustrated by a CN-A-K ternary diagram [*Fedo et al.*, 1995]. CN denotes
787 the mole weight of Na_2O and CaO* (CaO* represent the CaO associated with silicate, excluding
788 all the carbonate). A and K indicate the content of Al_2O_3 and K_2O respectively. Samples closer to
789 A are rich in kaolinite, chlorite and/or gibbsite (representing by Kao, Chl and Gib). CIA values
790 are also calculated and shown on the left side, with its values are correlated with the CN-A-K.
791 Samples from the delta have the lowest values of CIA and indicates high contents of CaO and
792 Na_2O and plagioclase. Abbreviations: sm (smectite), pl (plagioclase), ksp (K-feldspar), il (illite),
793 m (muscovite).
794

795 Figure 7. Plot of Th/U ratios versus U–Pb ages of concordant detrital zircons from the Paleogene
796 basins of NE Vietnam, SW Chinese basins and modern rivers (Yangtze at Shigu, Dadu, Yalong,
797 and the Red River at Hanoi, Yen Bai and Lao Cai). Th/U values >0.3 indicate the zircons having
798 an igneous origin whereas the values <0.1 represent the metamorphic zircons [*Maas et al.*, 1992].
799
800 Figure 8. Kernel density estimate (KDE) plots of detrital zircon U-Pb ages from A) newly
801 analyzed Paleogene sedimentary rocks from northern Vietnam, Neogene basins from along the
802 Red River Fault Zone [*Hoang et al.*, 2009], the Jianchuan Basin [*Wissink et al.*, 2016; *Yan et al.*,
803 2012] and from the Gulf of Tonkin/Qiongdongnan Basin [*Lei et al.*, 2019]. Jianchuan samples
804 from *Wissink et al.* [2016] are shown with their sample labels (Lim, Lij and Dali). Samples from
805 *Yan et al.* [2012] have no sample numbers. The new Jianchuan sample is labelled Shuange-18.
806 Vertical color bars indicate common peaks seen in East Asia and associated with certain
807 orogenic events and regions. B) KDE plots for the major rivers [*Clift et al.*, 2006b; *He et al.*,
808 2014; *Hoang et al.*, 2009] and primary basement source terrains from compilation of *He et al.*
809 [2014]. Indochina data is from *Nagy et al*. [2001], *Carter and Moss* [1999], *Carter and Bristow*
810 [2003] and *Carter et al*. [2001]. Hainan data is from *Xu et al*. [2016].
811
812 Figure 9. A) Multi-dimensional scalar (MDS) diagram of new U-Pb age spectra for the
813 Paleogene sedimentary rocks of NE Vietnam, showing how they compare to existing Neogene
814 sedimentary rocks in northern Vietnam close to the Red River [*Hoang et al.*, 2009], with
815 Paleogene sedimentary rocks in the Jianchuan Basin [*Wissink et al.*, 2016; *Yan et al.*, 2012], as
816 well as select major rivers [*Clift et al.*, 2006b; *He et al.*, 2014; *Hoang et al.*, 2009]. B) Associated
817 Shepherd plot.

818

819 Figure 10. Three-dimension MDS diagram of the Paleogene sedimentary rocks discussed in this
820 work together with the primary bedrock source terrains. MDS based on the K-S test D value
821 [*Saylor et al.*, 2018].

822

823 Figure 11. Calculated contributions from bedrock source terrains to sediments considered in this
824 study. Estimates based on the D value of the K-S test constrained end member mixing from
825 *Sundell and Saylor* [2017] are shown in black, while those derived from the V factor of the
826 Kuiper teset are shown in gray. Error bars show 1σ uncertainty. See Supplementary Table 1 for
827 numerical data.

828

829 Figure 12. Cumulative frequency plots showing the closeness of fit between the K-S derived
830 forward models (green) and the observed U-Pb age spectra of the sediment groups considered in
831 this study (black). Samples with large gaps between models and observation imply the influence
832 of additional sources not accounted for in this work.

833

834 Figure 13. Plot showing the similarity of the U-Pb zircon age spectra of the various Cenozoic
835 siliciclastic sedimentary rocks and major source terrains based on K-S testing [*Saylor and*
836 *Sundell*, 2016]..

837

838 Table 1. List of samples analyzed in this study together with their precise sampling locations and
839 rock type.

840

841 Table 2. Major and trace element analyses of some of the sediments from the Vietnamese basins
842 subjected to zircon U-Pb dating and that did not form part of the earlier *Wysocka et al*. [2018]
843 study.
844
845 Table 3. Analytical data for the zircon U-Pb analyses presented in this study.
846
847

References

Binh, N. B., N. N. Chau, N. V. Dien, P. M. Dat, N. B. Hoa, and N. Q. Lai (2003), Geological Map of Cao Bang's Sheet (1/25,000) Report on Geological Survey of Cao Bang-Ha Giang-Tuyen Quang Urbans (Cao Bang Urban). Union of Hydrogeology and Engineering Geology of Northern Vietnam, 1-187 pp, Department of Geology and Mineral of Vietnam, Hanoi.

Black, L. P., S. L. Kamo, I. S. Williams, R. Mundil, D. W. Davis, R. J. Korsch, and C. Foudoulis (2003), The application of SHRIMP to Phanerozoic geochronology; a critical appraisal of four zircon standards, *Chemical Geology*, *200*(1-2), 171-188.

Böhme, M., M. Aiglstorfer, A. P.-O., E. Appel, P. Havlik, G. Métais, L. T. Phuc, S. Schneider, F. Setzer, R. Tappert, D. N. Tran, D. Uhl, and J. Prieto (2013), Na Duong (northern Vietnam) – an exceptional window into Eocene ecosystems from Southeast Asia, *Zitteliana*, *53*, 120–167.

Böhme, M., J. Prieto, S. Schneider, N. V. Hung, D. D. Quang, and D. N. Tran (2011), The Cenozoic on-shore basins of Northern Vietnam: Biostratigraphy, vertebrate and invertebrate faunas, *Journal of Asian Earth Sciences*, *40*, 672–687.

Brookfield, M. E. (1998), The evolution of the great river systems of southern Asia during the Cenozoic India-Asia collision; rivers draining southwards, *Geomorphology*, *22*(3-4), 285-312.

Carter, A., and C. S. Bristow (2003), Linking hinterland evolution and continental basin sedimentation by using detrital zircon thermochronology; a study of the Khorat Plateau basin, eastern Thailand, *Basin Research*, *15*, 271–285.

Carter, A., and P. D. Clift (2008), Was the Indosinian orogeny a Triassic mountain building or thermotectonic reactivation event?, *Comptes Rendues de l'Academie Scientifique, Geoscience*, *340*, 83–93.

Carter, A., and S. J. Moss (1999), Combined detrital-zircon fission-track and U-Pb dating: a new approach to understanding hinterland evolution, *Geology*, *27*, 235–238.

Carter, A., D. Roques, C. Bristow, and P. D. Kinny (2001), Understanding Mesozoic accretion in Southeast Asia: Significance of Triassic thermotectonism (Indosinian orogeny) in Vietnam, *Geology*, *29*, 211–214.

878 Chen, Y., M. Yan, X. Fang, C. Song, W. Zhang, J. Zan, Z. Zhang, B. Li, Y. Yang, and D. Zhang
879 (2017), Detrital zircon U–Pb geochronological and sedimentological study of the Simao
880 Basin, Yunnan: Implications for the Early Cenozoic evolution of the Red River, *Earth and*
881 *Planetary Science Letters*, *476*, 22-33, doi:10.1016/j.epsl.2017.07.025.
882 Clark, M. K., L. M. Schoenbohm, L. H. Royden, K. X. Whipple, B. C. Burchfiel, X. Zhang, W.
883 Tang, E. Wang, and L. Chen (2004), Surface uplift, tectonics, and erosion of eastern Tibet
884 from large-scale drainage patterns, *Tectonics*, *23, TC1006*, doi:10.1029/2002TC001402.
885 Clift, P. D., J. Blusztajn, and D. A. Nguyen (2006a), Large-scale drainage capture and surface
886 uplift in eastern Tibet-SW China before 24 Ma inferred from sediments of the Hanoi Basin,
887 Vietnam, *Geophysical Research Letters*, *33*(L19403), doi:10.1029/2006GL027772.
888 Clift, P. D., A. Carter, I. H. Campbell, M. Pringle, K. V. Hodges, N. V. Lap, and C. M. Allen
889 (2006b), Thermochronology of mineral grains in the Song Hong and Mekong Rivers,
890 Vietnam, *Geophysics, Geochemistry, Geosystems*, *7*(Q10005),
891 doi:10.1029/2006GC001336.
892 Clift, P. D., V. L. Hoang, R. Hinton, R. Ellam, R. Hannigan, M. T. Tan, and D. A. Nguyen
893 (2008), Evolving East Asian river systems reconstructed by trace element and Pb and Nd
894 isotope variations in modern and ancient Red River-Song Hong sediments, *Geochemistry*
895 *Geophysics Geosystems*, *9*(Q04039), doi:10.1029/2007GC001867.
896 Cuong, N. T., L. V. Duc, D. Q. Huy, H. V. Khoa, T. T. Hoa, and N. V. Phong (2000), Geological
897 and mineral resources map of Cao Bang-Dong Khe Sheet, Northeastern Geological
898 Division. Department of Geology and Mineral of Vietnam, Hanoi.
899 Ducrocq, S., M. Benammi, O. Chavasseau, Y. Chaimanee, K. Suraprasit, P. D. Pha, V. L.
900 Phuong, P. V. Phach, and J.-J. Jaeger (2015), New anthracotheres (Cetartiodactyla,
901 Mammalia) from the Paleogene of northeastern Vietnam: biochronological implications,
902 *Journal of Vertebrate Paleontology*, *35*(3), e929139.
903 Fedo, C. M., H. W. Nesbitt, and G. M. Young (1995), Unraveling the effects of potassium
904 metasomatism in sedimentary rocks and paleosols, with implications for paleoweathering
905 conditions and provenance, *Geology*, *23*, 921–924.
906 Fromaget, J., E. Saurin, and H. Fontaine (1971), Geological Map of Vietnam, Cambodia and
907 Laos, National Geographic Directorate of Vietnam, Dalat.

908 Fyhn, M. B. W., T. D. Cuong, B. H. Hoang, J. Hovikoski, M. Olivarius, N. Q. Tuan, N. T. Tung,
909 N. T. Huyen, T. X. Cuong, H. P. Nytoft, I. Abatzis, and L. H. Nielsen (2018), Linking
910 Paleogene Rifting and Inversion in the Northern Song Hong and Beibuwan Basins,
911 Vietnam, With Left-Lateral Motion on the Ailao Shan-Red River Shear Zone, *Tectonics*,
912 *37*(8), 2559-2585, doi:10.1029/2018TC005090.
913 Gilley, L. D., T. M. Harrison, P. H. Leloup, F. J. Ryerson, O. M. Lovera, and J. H. Wang (2003),
914 Direct dating of left-lateral deformation along the Red River shear zone, China and
915 Vietnam, *Journal of Geophysical Research*, *108*(2127), doi:10.1029/2001JB001726.
916 Gourbet, L., P. H. Leloup, J.-L. Paquette, P. Sorrel, G. Maheo, G. Wang, X. Yadong, K. Cao, P.-
917 O. Antoine, I. Eymard, W. Liu, H. Lu, A. Replumaz, M.-L. Chevalier, Z. Kexin, W. Jing,
918 and T. Shen (2017), Reappraisal of the Jianchuan Cenozoic basin stratigraphy and its
919 implications on the SE Tibetan plateau evolution, *Tectonophysics*, *700-701*, 162-179,
920 doi:10.1016/j.tecto.2017.02.007.
921 Griffin, W. (2008), GLITTER: data reduction software for laser ablation ICP-MS, *Laser*
922 *Ablation ICP-MS in the Earth Sciences: Current practices and outstanding issues*, 308-
923 311.
924 Harley, S. L., N. M. Kelly, and A. Möller (2007), Zircon behaviour and the thermal histories of
925 mountain chains, *Elements*, *3*, 25–30.
926 He, M., H. Zheng, B. Bookhagen, and P. D. Clift (2014), Controls on erosion intensity in the
927 Yangtze River basin tracked by U-Pb detrital zircon dating, *Earth Science Reviews*, *136*,
928 121–140, doi:10.1016/j.earscirev.2014.05.014.
929 Hoang, L. V., P. D. Clift, D. Mark, H. Zheng, and M. T. Tan (2010), Ar-Ar Muscovite dating as
930 a constraint on sediment provenance and erosion processes in the Red and Yangtze River
931 systems, SE Asia, *Earth and Planetary Science Letters*, *295*, 379–389,
932 doi:10.1016/j.epsl.2010.04.012.
933 Hoang, L. V., F. Y. Wu, P. D. Clift, A. Wysocka, and A. Swierczewska (2009), Evaluating the
934 evolution of the Red River system based on in-situ U-Pb dating and Hf isotope analysis of
935 zircons, *Geochemistry Geophysics Geosystems*, *10*(Q11008), doi:10.1029/2009GC002819.
936 Hoke, G. D., J. Liu-Zeng, and M. T. Hren (2014), Stable isotopes reveal high southeast Tibetan
937 Plateau margin since the Paleogene, *Earth and Planetary Science Letters*, *394*, 270–278,
938 doi:10.1016/j.epsl.2014.03.007.

939 Johnson, D., P. Hooper, and R. Conrey (1999), XRF Method XRF Analysis of Rocks and
940 Minerals for Major and Trace Elements on a Single Low Dilution Li-Tetraborate Fused
941 Bead, *Adv. X-ray anal*, *41*, 843-867.
942 Kong, P., D. E. Granger, F.-Y. Wu, M. W. Caffee, Y.-J. Wang, X.-T. Zhao, and Y. Zheng
943 (2009), Cosmogenic nuclide burial ages and provenance of the Xigeda paleo-lake:
944 Implications for evolution of the Middle Yangtze River, *Earth and Planetary Science*
945 *Letters*, *278*(1-2,), 131-141.
946 Kong, P., Y. Zheng, and M. W. Caffee (2012), Provenance and time constraints on the formation
947 of the first bend of the Yangtze River, *Geochemistry, Geophysics, Geosystems*,
948 *13*(Q06017), doi:10.1029/2012GC004140.
949 Lei, C., P. D. Clift, J. Ren, J. Ogg, and C. Tong (2019), A rapid shift in the sediment routing
950 system of lower-upper Oligocene strata in the Qongdongnnan basin (Xisha Trough),
951 Northwest south China Sea, *Marine and Petroleum Geology*,
952 doi:10.1016/j.marpetgeo.2019.03.012.
953 Leloup, P. H., N. Arnaud, R. Lacassin, J. R. Kienast, T. M. Harrison, T. Phan Trong, A.
954 Replumaz, and P. Tapponnier (2001), New constraints on the structure, thermochronology,
955 and timing of the Ailao Shan-Red River shear zone, SE Asia, *Journal of Geophysical*
956 *Research*, *106*(B4), 6657-6671.
957 Lepvrier, C., H. Maluski, V. T. Vu, A. Leyreloup, T. T. Phan, and N. V. Vuong (2004), The
958 Early Triassic Indosinian orogeny in Vietnam (Truong Son Belt and Kontum Massif);
959 implications for the geodynamic evolution of Indochina, *Tectonophysics*, *393*, 87-118.
960 Liu, S., D. Zhong, and G. Wu (1998), Jinggu-Zhenyuan transpressional basin during continent-
961 continent collision of early Tertiary in southwest Yunnan, China, *Scientia Geologica*
962 *Sinica (in Chinese)*, *33*(1), 1-8.
963 Lupker, M., C. France-Lanord, V. Galy, J. Lave, J. Gaillardet, A. P. Gajured, C. Guilmette, M.
964 Rahman, S. K. Singh, and R. Sinha (2012), Predominant floodplain over mountain
965 weathering of Himalayan sediments (Ganga basin), *Geochimica et Cosmochimica Acta*, *84*,
966 410-432.
967 Maas, R., P. D. Kinny, I. S. Williams, D. O. Froude, and W. Compston (1992), The Earth's
968 oldest known crust: A geochronological and geochemical study of 3900–4200 Ma old

969 detrital zircons from Mt. Narryer and Jack Hills, Western Australia, *Geochimica et*
970 *Cosmochimica Acta*, *56*(3), 1281-1300, doi:10.1016/0016-7037(92)90062-N.
971 McPhillips, D., G. D. Hoke, J. Liu-Zeng, P. R. Bierman, D. H. Rood, and S. Niedermann (2016),
972 Dating the incision of the Yangtze River gorge at the First Bend using three-nuclide burial
973 ages, *Geophysical Research Letters*, *43*(1), 101-110, doi:10.1002/2015GL066780.
974 Metcalfe, I. (1996), Pre-Cretaceous evolution of SE Asian terranes, in *Tectonic evolution of SE*
975 *Asia*, edited by R. Hall and D. J. Blundell, pp. 97–122, Geological Society London.
976 Morley, C. K. (2002), A tectonic model for the Tertiary evolution of strike-slip faults and rift
977 basins in SE Asia, *Tectonophysics*, *347*(4), 189-215.
978 Nagy, E. A., H. Maluski, C. Lepvrier, U. Schärer, T. T. Phan, A. Leyreloup, and V. T. Vu
979 (2001), Geodynamic significance of the Kontum Massif in central Vietnam; composite
980 40Ar/39Ar and U-Pb ages from Paleozoic to Triassic, *Journal of Geology*, *109*, 755–770.
981 Nesbitt, H. W., G. Markovics, and R. C. Price (1980), Chemical processes affecting alkalis and
982 alkaline earths during continental weathering, *Geochimica et Cosmochimica Acta*, *44*,
983 1659–1666.
984 Pearce, N. J. G., W. T. Perkins, J. A. Westgate, M. P. Gorton, S. E. Jackson, C. R. Neal, and S.
985 P. Chenery (1997), A compilation of new and published major and trace element data for
986 NIST SRM 610 and NIST SRM 612 glass reference materials, *Geostandards Newsletter-*
987 *the Journal of Geostandards and Geoanalysis*, *21*(1), 115-144.
988 Pubellier, M., C. Rangin, P. V. Phach, B. C. Que, D. T. Hung, and C. L. Sang (2003), The Cao
989 Bang-Tien Yen Fault: Implications on the relationships between the Red River Fault and
990 the South China Coastal Belt, *Advances in Natural Sciences*, *4*(4), 347-361.
991 Pullen, A., M. Ibanez-Mejıa, G. E. Gehrels, J. C. Ibanez-Mejıa, and M. Pecha (2014), What
992 happens when n¼ 1000? Creating large-n geochronological datasets with LA-ICP-MS for
993 geologic investigations, *Journal of Analytical Atomic Spectrometry*, *29*, 971-980,
994 doi:10.1039/c4ja00024b.
995 Rangin, C., P. Huchon, X. L. Pichon, H. Bellon, C. Lepvrier, D. Roques, N. D. Hoe, and P. V.
996 Quynh (1995), Cenozoic deformation of central and south Vietnam, *Tectonophysics*,
997 *251*(1-4), 179-196, doi:10.1016/0040-1951(95)00006-2

998 Replumaz, A., and P. Tapponnier (2003), Reconstruction of the deformed collision zone between
999 India and Asia by backward motion of lithospheric blocks, *Journal of Geophysical*
1000 *Research*, *108, 2285*(B6), doi:10.1029/2001JB000661.
1001 Richardson, N. J., A. L. Densmore, D. Seward, M. Wipf, and L. Yong (2010), Did incision of the
1002 Three Gorges begin in the Eocene?, *Geology*, *38*(6), 551–554, doi: 10.1130/G30527.1.
1003 Royden, L. H., B. C. Burchfiel, and R. D. van der Hilst (2008), The Geological Evolution of the
1004 Tibetan Plateau, *Science*, *321*(5892), 1054-1058, doi:10.1126/science.1155371.
1005 Saylor, J. E., J. C. Jordan, K. E. Sundell, X. Wang, S. Wang, and T. Deng (2018), Topographic
1006 growth of the Jishi Shan and its impact on basin and hydrology evolution, NE Tibetan
1007 Plateau, *Basin Research*, *30*(3), 544-563, doi:10.1111/bre.12264.
1008 Saylor, J. E., and K. E. Sundell (2016), Quantifying comparison of large detrital geochronology
1009 data sets, *Geosphere*, *12*(1), 203-220, doi:10.1130/ges01237.1.
1010 Schoenbohm, L. M., B. C. Burchfiel, L. Chen, and J. Yin (2005), Exhumation of the Ailao Shan
1011 shear zone recorded by Cenozoic sedimentary rocks, Yunnan Province, China, *Tectonics*,
1012 *24*(TC6015), 18, doi: 10.1029/2005TC001803.
1013 Schoenbohm, L. M., B. C. Burchfiel, L. Chen, and J. Yin (2006), Miocene to present activity
1014 along the Red River Fault, China, in the context of continental extrusion, upper-crustal
1015 rotation, and lower-crustal flow, *Geological Society of America Bulletin*, *118*(5-6), 672-
1016 688.
1017 Schulz, B., R. Klemd, and H. Braetz (2006), Host rock compositional controls on zircon trace
1018 element signatures in metabasites from the Austroalpine basement, *Geochimica et*
1019 *Cosmochimica Acta*, *70*, 697–710.
1020 Searle, M. P., C. K. Morley, D. J. Waters, N. J. Gardiner, U. K. Htun, Than Than Nu, and L. J.
1021 Robb (2017), Chapter 12 Tectonic and metamorphic evolution of the Mogok
1022 Metamorphic and Jade Mines belts and ophiolitic terranes of Burma (Myanmar),
1023 *Geological Society, London, Memoirs*, *48*(1), 261-293, doi:10.1144/m48.12.
1024 Shen, X., Y. Tian, D. Li, S. Qin, P. Vermeesch, and J. Schwanethal (2016), Oligocene-Early
1025 Miocene river incision near the first bend of the Yangze River: Insights from apatite (U-
1026 Th-Sm)/He thermochronology, *Tectonophysics*, *687*, 223-231,
1027 doi:10.1016/j.tecto.2016.08.006.

1028 Singh, M., M. Sharma, and H. J. Tobschall (2005), Weathering of the Ganga alluvial plain,
1029 northern India: implications from fluvial geochemistry of the Gomati River, *Applied*
1030 *Geochemistry*, *20*, 1-21.
1031 Sláma, J., J. Košler, D. J. Condon, J. L. Crowley, A. Gerdes, J. M. Hanchar, M. S. A. Horstwood,
1032 G. A. Morris, L. Nasdala, N. Norberg, U. Schaltegger, B. Schoene, M. N. Tubrett, and M.
1033 J. Whitehouse (2008), Plezovice zircon A new natural reference material for U–Pb and Hf
1034 isotopic microanalysis, *Chemical Geology*, *249*, 1-35, doi:10.1016/j.chemgeo.2007.11.005.
1035 Sundell, K., and J. E. Saylor (2017), Unmixing detrital geochronology age distributions,
1036 *Geochemistry Geophysics Geosystems*, *18*, 2872–2886.
1037 Tapponnier, P., R. Lacassin, P. H. Leloup, U. Schaerer, Z. Dalai, W. Haiwei, L. Xiaohan, J.
1038 Shaocheng, Z. Lianshang, and Z. Jiayou (1990), The Ailao Shan/Red River metamorphic
1039 belt; Tertiary left-lateral shear between Indochina and South China, *Nature*, *343*(6257),
1040 431-437.
1041 Taylor, S. R., and S. M. McLennan (1995), The geochemical evolution of the continental crust,
1042 *Reviews of Geophysics*, *33*, 241–265.
1043 Vermeesch, P. (2004), How many grains are needed for a provenance study?, *Earth and*
1044 *Planetary Science Letters*, *224*, 351–441.
1045 Vermeesch, P. (2012), On the visualisation of detrital age distributions, *Chemical Geology*, *312–*
1046 *313*, 190–194, doi:10.1016/j.chemgeo.2012.04.021.
1047 Vermeesch, P., A. Resentini, and E. Garzanti (2016), An R package for statistical provenance
1048 analysis, *Sedimentary Geology*, *336*, 14-25, doi:10.1016/j.sedgeo.2016.01.009.
1049 Wang, C., J. Dai, X. Zhao, Y. Li, S. A. Graham, D. He, B. Ran, and J. Meng (2014), Outward-
1050 growth of the Tibetan Plateau during the Cenozoic: A review, *Tectonophysics*, *621*, 1-43,
1051 doi:10.1016/j.tecto.2014.01.036.
1052 Wang, E., E. Kirby, K. P. Furlong, M. v. Soest, G. Xu, X. Shi, P. J. J. Kamp, and K. V. Hodges
1053 (2012), Two-phase growth of high topography in eastern Tibet during the Cenozoic,
1054 *Nature Geoscience*, *5*, 640–645, doi:10.1038/ngeo1538.
1055 Wei, H.-H., E. Wang, G.-L. Wu, and K. Meng (2016), No sedimentary records indicating
1056 southerly flow of the paleo-Upper Yangtze River from the First Bend in southeastern
1057 Tibet, *Gondwana Research*, *32*, 93-104, doi:10.1016/j.gr.2015.02.006.

1058 Weislogel, A. L., S. A. Graham, E. Z. Chang, J. L. Wooden, and G. Gehrels (2010), Detrital
1059 zircon provenance from three turbidite depocenters of the Middle-Upper Triassic Songpan-
1060 Ganzi complex, central China: Record of collisional tectonics, erosional exhumation, and
1061 sediment production, *Geological Society of America Bulletin*, *122*, 2041-2062.
1062 Weislogel, A. L., S. A. Graham, E. Z. Chang, J. L. Wooden, G. E. Gehrels, and H. Yang (2006),
1063 Detrital zircon provenance of the Late Triassic Songpan-Ganzi complex: Sedimentary
1064 record of collision of the North and South China blocks, *Geology*, *34*, 97-100.
1065 West, A. J., A. Galy, and M. J. Bickle (2005), Tectonic and climatic controls on silicate
1066 weathering, *Earth and Planetary Science Letters*, *235*, 211–228, doi:
1067 10.1016/j.epsl.2005.03.020.
1068 Wiedenbeck, M., J. M. Hanchar, W. H. Peck, P. Sylvester, J. Valley, M. Whitehouse, A. Kronz,
1069 Y. Morishita, L. Nasdala, and J. Fiebig (2004), Further characterisation of the 91500 zircon
1070 crystal, *Geostandards and Geoanalytical Research*, *28*(1), 9-39.
1071 Wissink, G. K., G. D. Hoke, C. N. Garzione, and J. Liu-Zeng (2016), Temporal and spatial
1072 patterns of sediment routing across the southeast margin of the Tibetan Plateau: Insights
1073 from detrital zircon, *Tectonics*, *35*, doi:10.1002/ 2016TC004252.
1074 Wysocka, A. (2009), Sedimentary environments of the Neogene basins associated with the Cao
1075 Bang – Tien Yen Fault, NE Vietnam, *Acta Geologica Polonica*, *59*, 45-69.
1076 Wysocka, A., D. P. Pha, D. E., U. Czarniecka, D. V. Thang, F. A., N. Q. Cuong, D. M. Tuan, N.
1077 X. Huyen, and H. V. Tha (2018), New data on the continental deposits from the Cao Bang
1078 Basin (Cao Bang-Tien Yen Fault Zone, NE Vietnam) – biostratigraphy, provenance and
1079 facies pattern, *Acta Geologica Polonica*, *68*(4), 689–709, doi:10.1515/agp-2018-0037.
1080 Xu, Y., C. Y. Wang, and T. Zhao (2016), Using detrital zircons from river sands to constrain
1081 major tectono-thermal events of the Cathaysia Block, SE China, *Journal of Asian Earth*
1082 *Sciences*, *124*, 1–13, doi:10.1016/j.jseaes.2016.04.012.
1083 Yan, Y., A. Carter, C. Y. Huang, L. S. Chan, X. Q. Hu, and Q. Lan (2012), Constraints on
1084 Cenozoic regional drainage evolution of SW China from the provenance of the Jianchuan
1085 Basin, *Geophysics Geochemistry Geosystems*, *13*(Q03001), doi:10.1029/2011GC003803.
1086 Yan, Y., A. Carter, C. Palk, S. Brichau, and X. Hu (2011), Understanding sedimentation in the
1087 Song Hong–Yinggehai Basin, South China Sea, *Geochemistry, Geophysics, Geosystems*,
1088 *12*(6), doi:10.1029/2011GC003533.

Yunnan Bureau of Geology and Mineral Resources (1990), 1:200000 regional map series and accompanying reports, 728 pp.

Zhang, Y., D. Zhang, and S. Liu (1996), Stratigraphy (Lithostratic) of Yunnan Province, *China University of Geosciences Press, Wuhan*, 1-379.

Zhang, Z., S. Tyrrell, C. a. Li, J. S. Daly, X. Sun, and Q. Li (2014), Pb isotope compositions of detrital K-feldspar grains in the upper-middle Yangtze River system: Implications for sediment provenance and drainage evolution, *Geochemistry, Geophysics, Geosystems*, *15*(7), 2765-2779, doi:10.1002/2014GC005391.

Zheng, H., P. D. Clift, R. Tada, J. T. Jia, M. Y. He, and P. Wang (2013), A Pre-Miocene Birth to the Yangtze River, *Proceedings of the National Academy of Sciences*, 1-6, doi:10.1073/pnas.1216241110.

Figure 1.

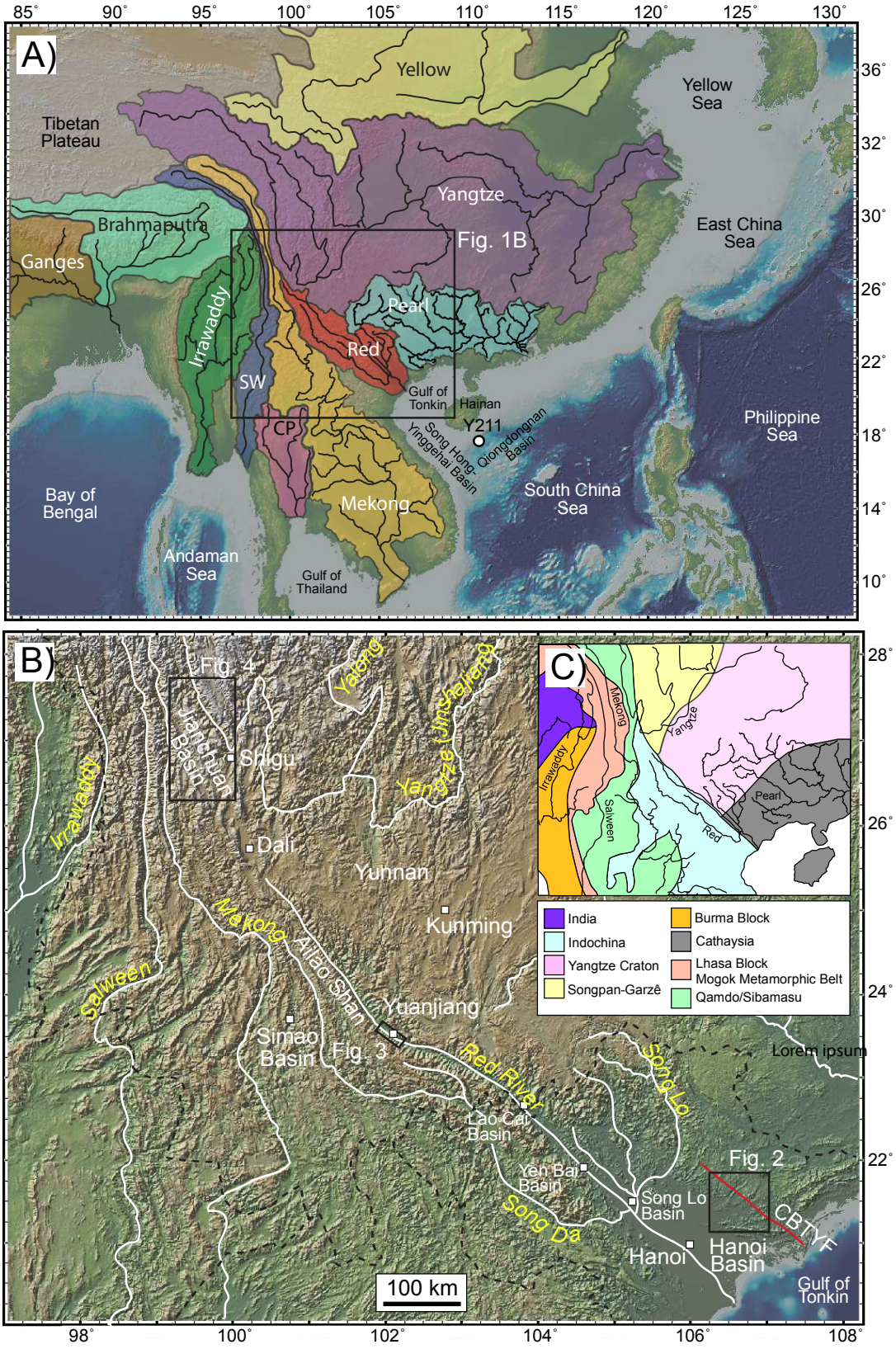

Figure 1
Clift et al.

Figure 2.

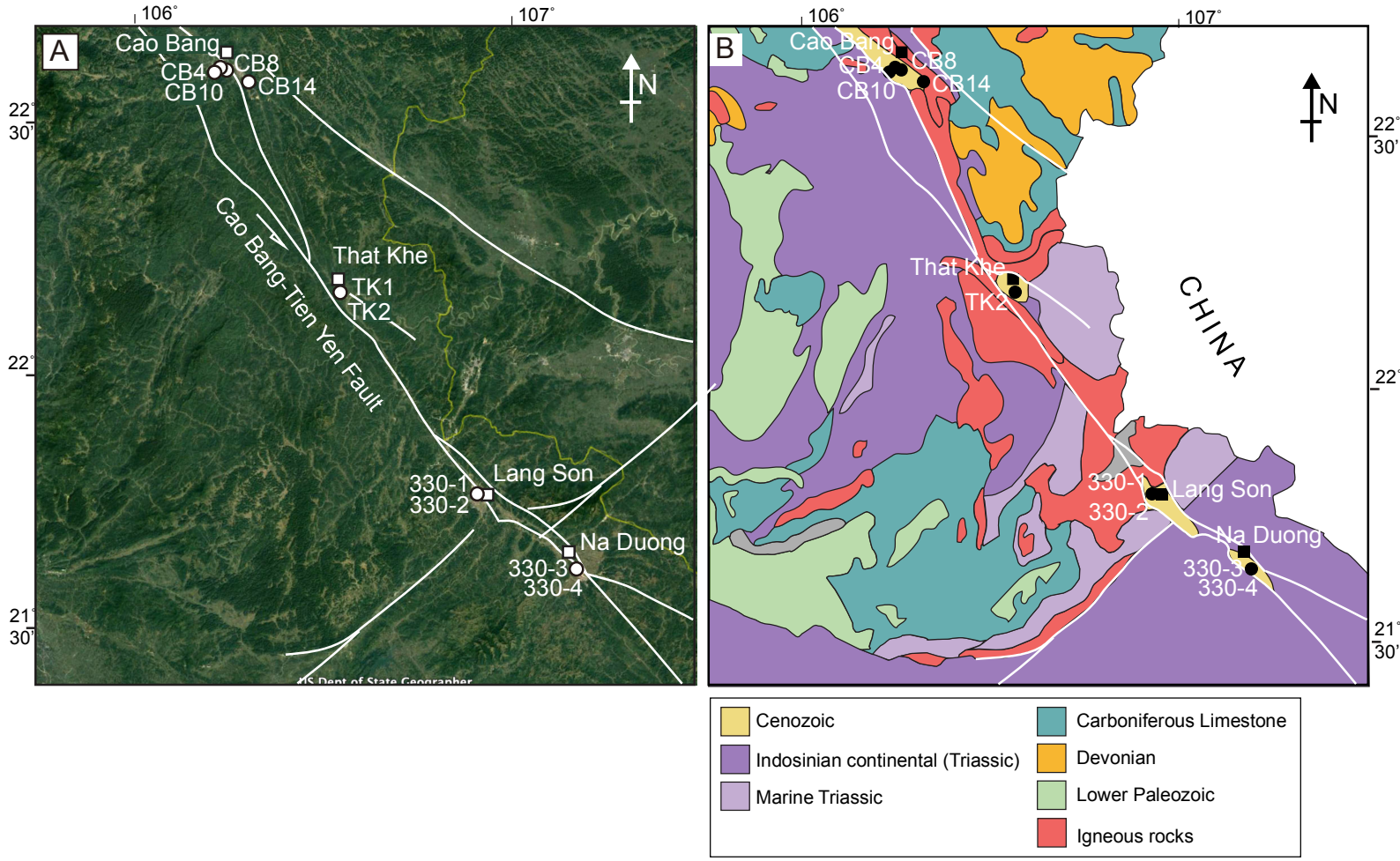

Figure 2
Clift et al.

Figure 3.

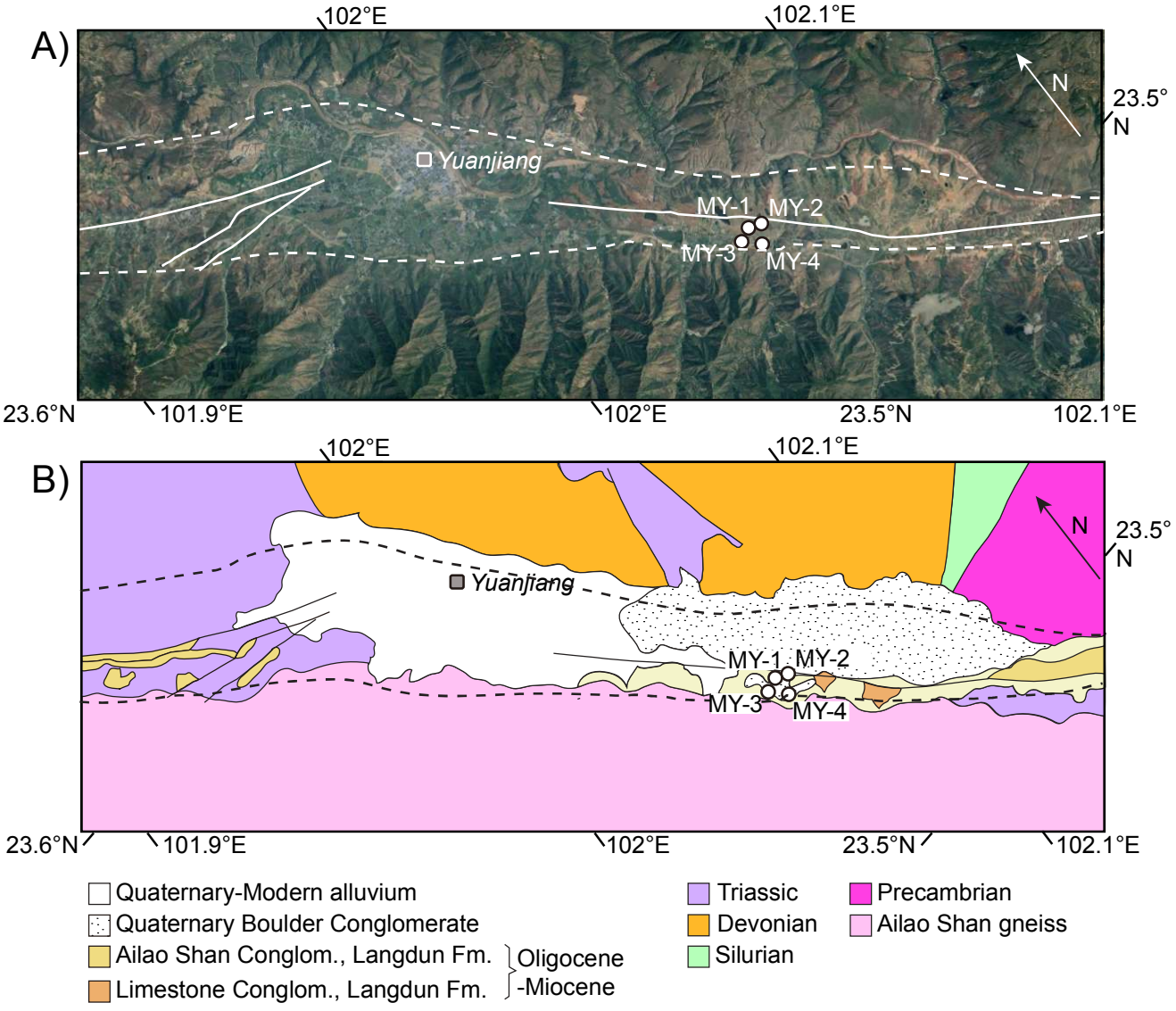
A)
102°E
102.1°E
N
23.5°N
Yuanjiang
MY-1
MY-2
MY-3
MY-4
23.6°N
101.9°E
102°E
23.5°N
102.1°E
B)
102°E
102.1°E
N
23.5°N
Yuanjiang
MY-1
MY-2
MY-3
MY-4
23.6°N
101.9°E
102°E
23.5°N
102.1°E
Quaternary-Modern alluvium
Quaternary Boulder Conglomerate
Ailao Shan Conglom., Langdun Fm.
Limestone Conglom., Langdun Fm.
Oligocene -Miocene
Triassic
Devonian
Silurian
Precambrian
Ailao Shan gneiss

Figure 4.

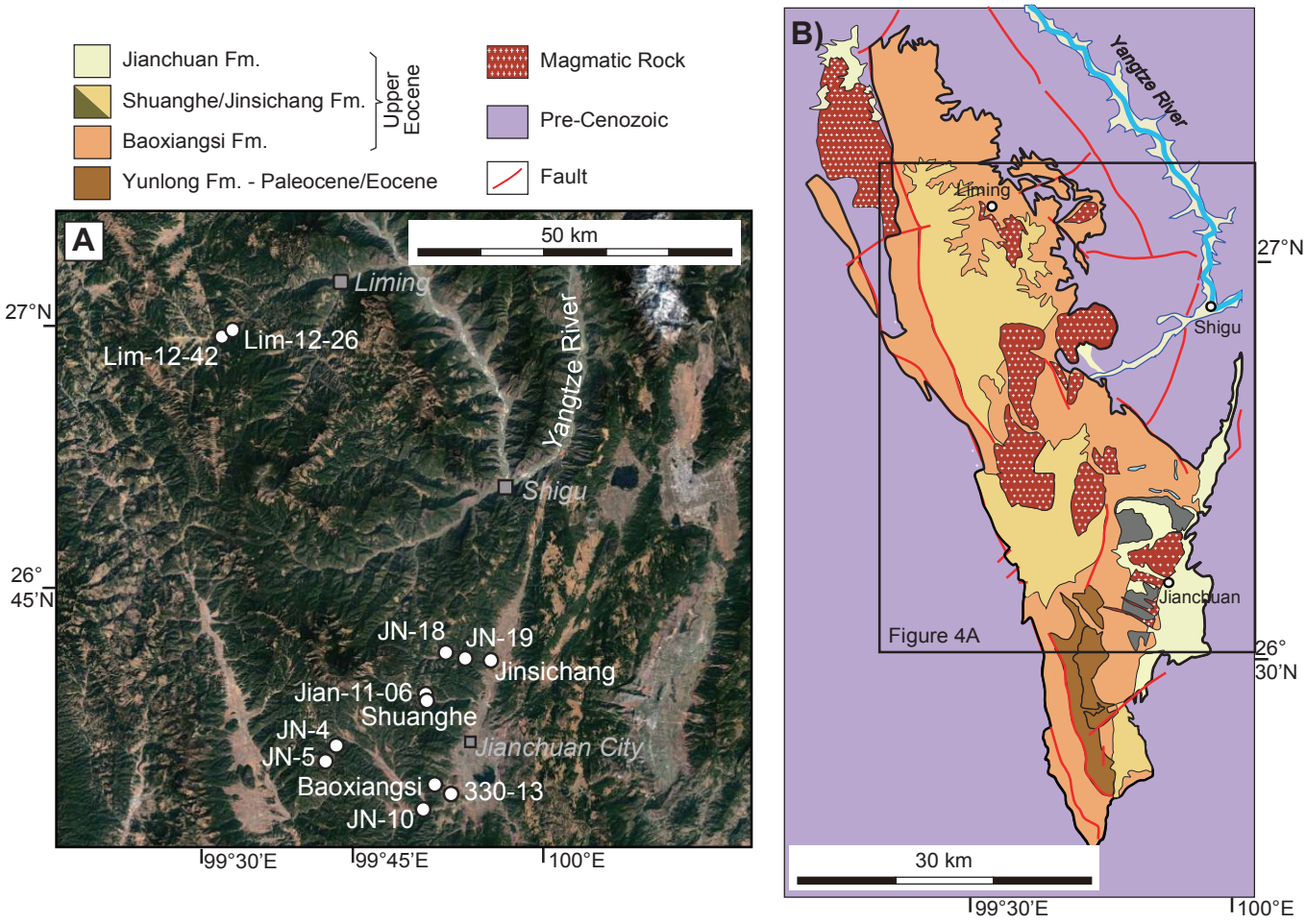
Jianchuan Fm.
Shuanghe/Jinsichang Fm.
Baoxiangsi Fm.
Yunlong Fm. - Paleocene/Eocene
Upper Eocene
Magmatic Rock
Pre-Cenozoic
Fault
A
50 km
Liming
Lim-12-26
Lim-12-42
Yangtze River
Shigu
JN-18
JN-19
Jinsichang
Jian-11-06
Shuanghe
JN-4
JN-5
Jianchuan City
Baoxiangsi
330-13
JN-10
27°N
26° 45'N
99°30'E
99°45'E
100°E
B)
Yangtze River
Liming
Shigu
Jianchuan
Figure 4A
27°N
26° 30'N
30 km
99°30'E
100°E

Figure 5.

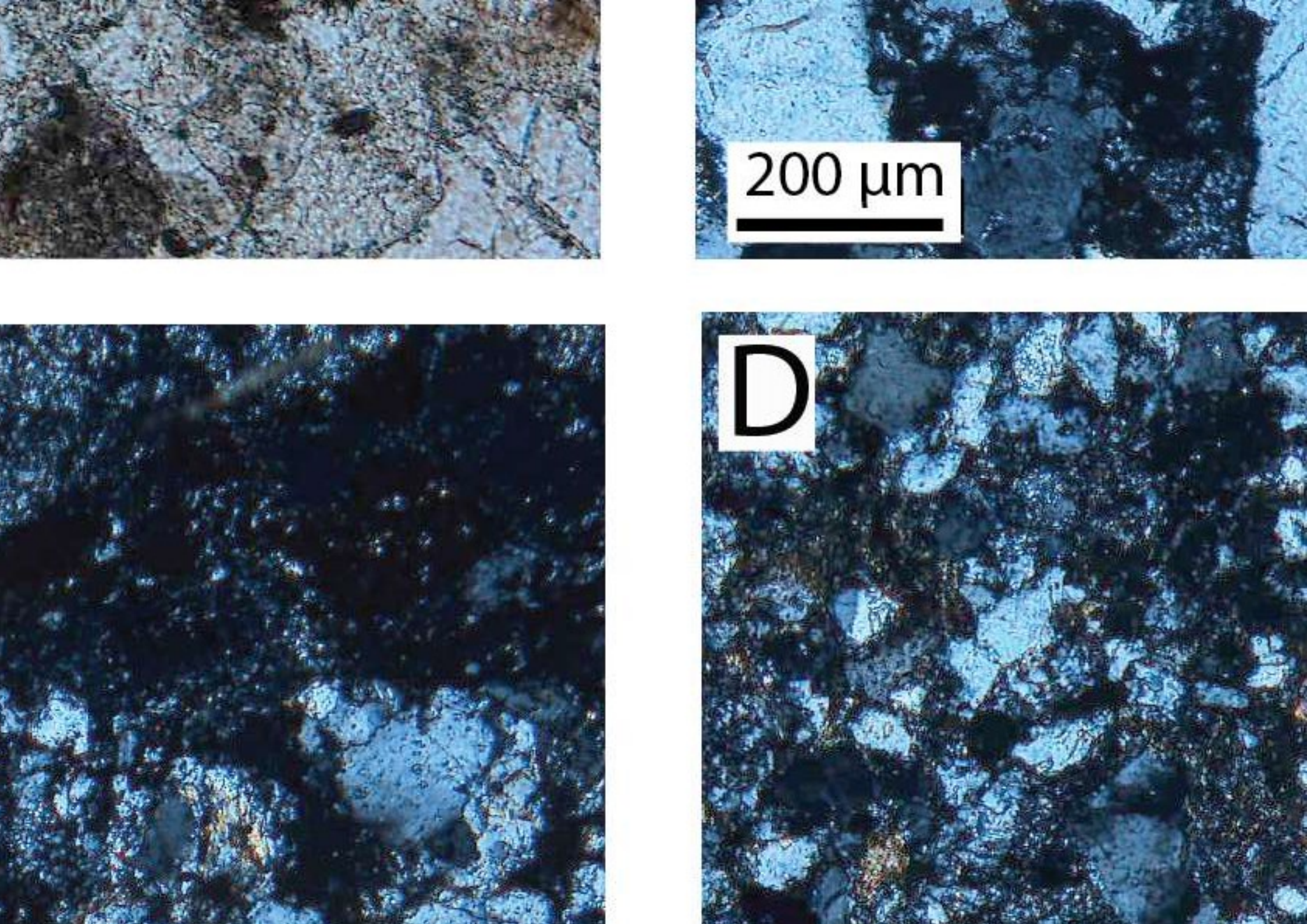
200 µm
D

Figure 6.

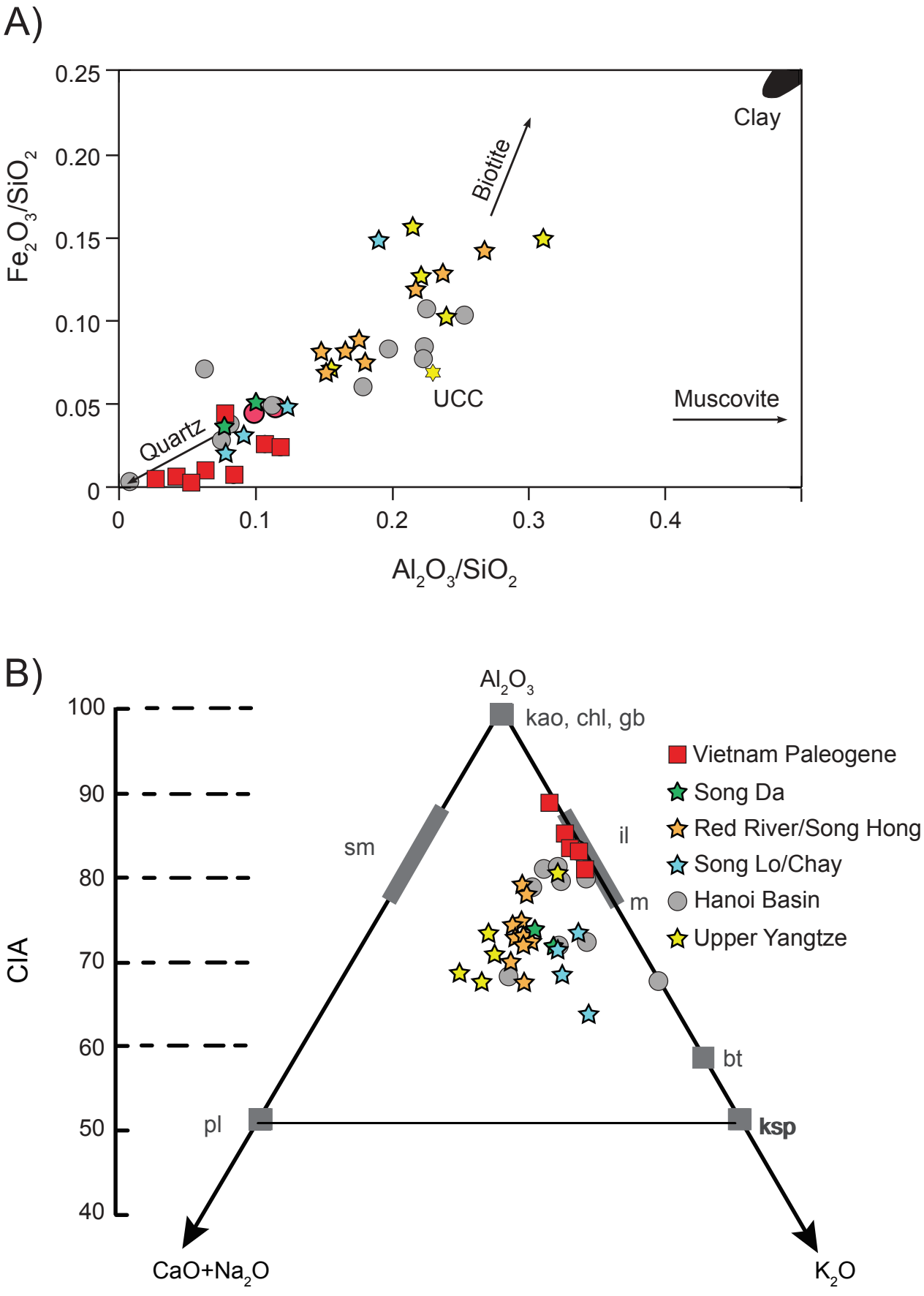

Figure 6
Clift et al.

Figure 7.

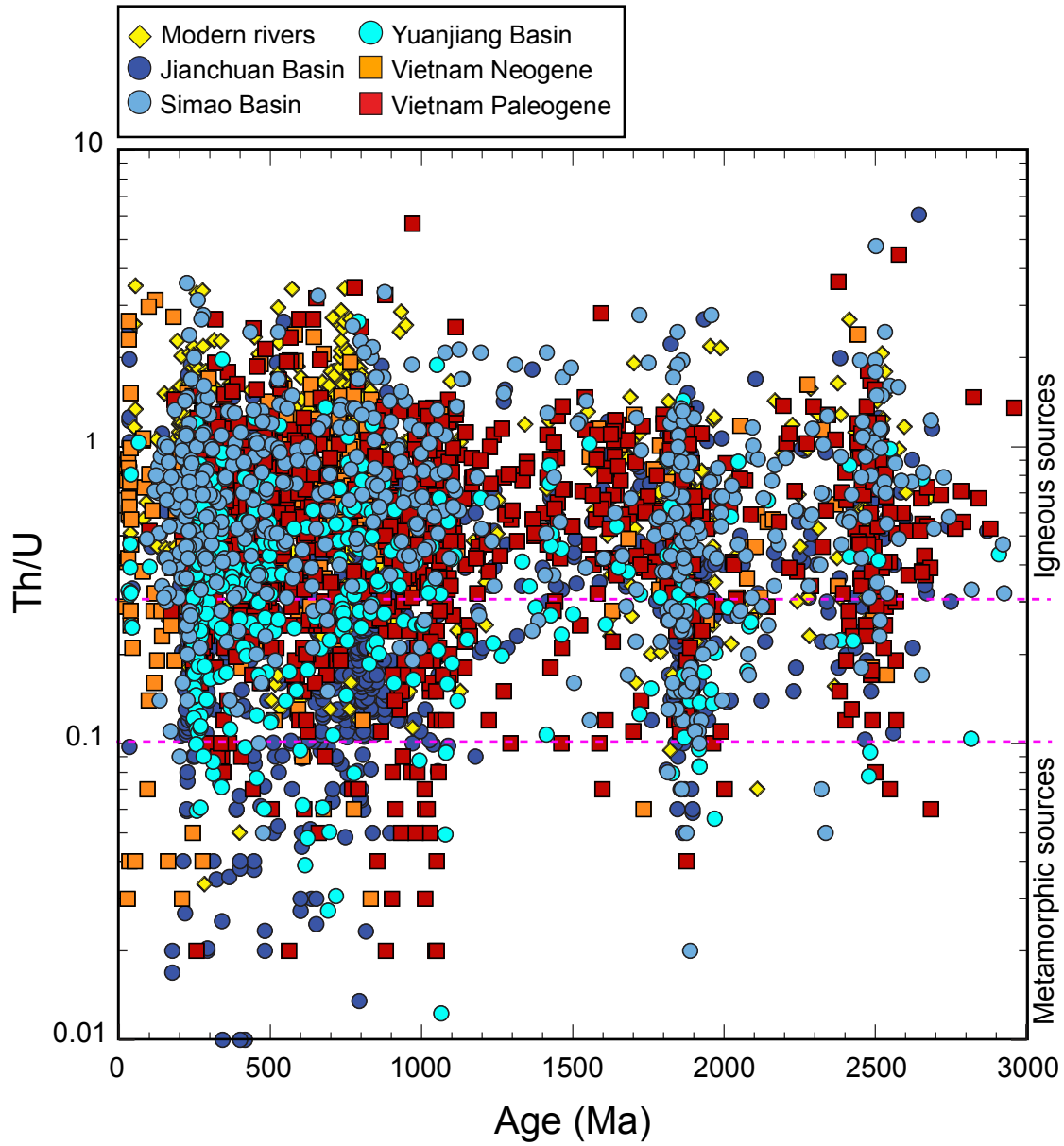
Modern rivers
Jianchuan Basin
Simao Basin
Yuanjiang Basin
Vietnam Neogene
Vietnam Paleogene
10
1
0.1
0.01
Th/U
0
500
1000
1500
2000
2500
3000
Age (Ma)
Igneous sources
Metamorphic sources

Figure 8.

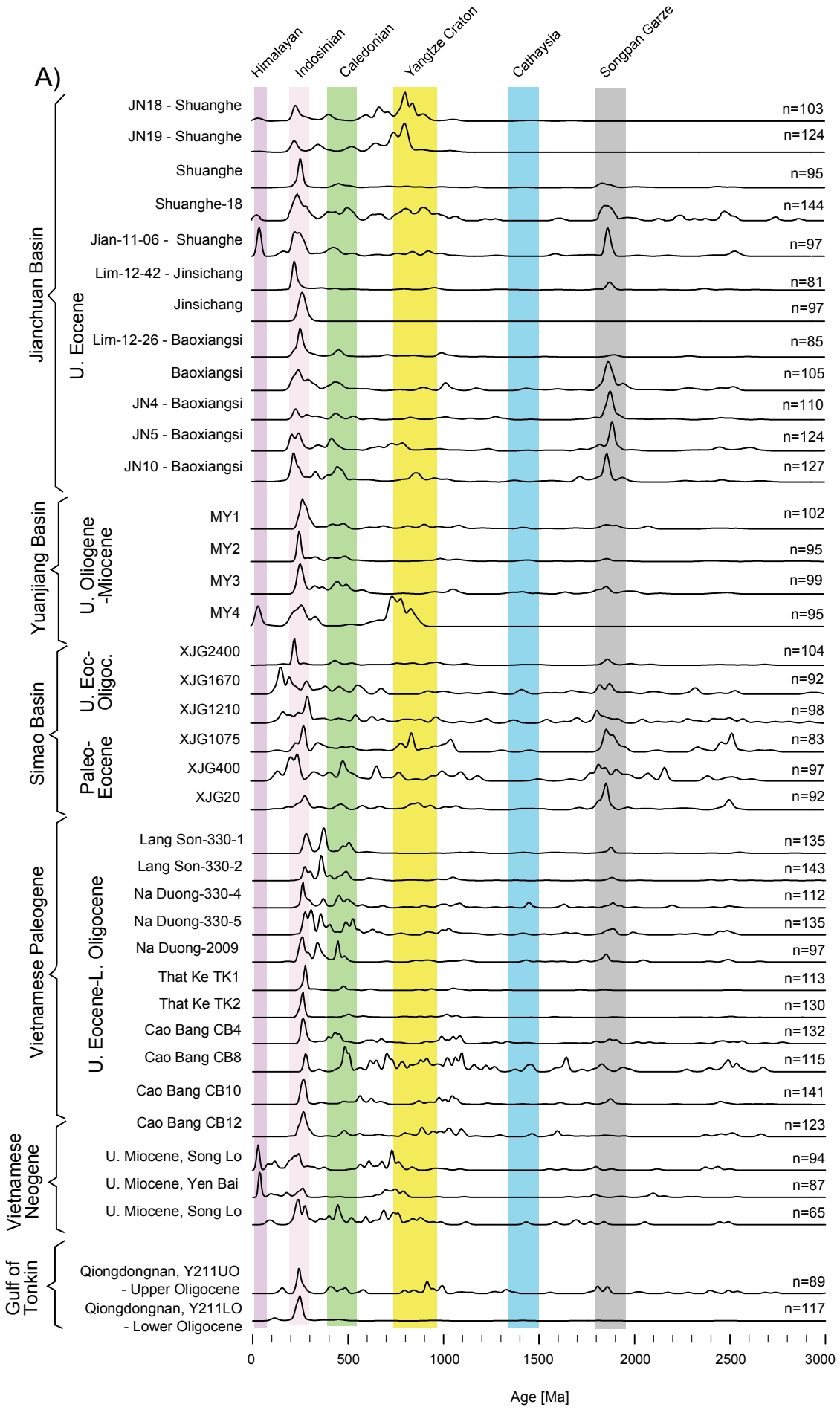
A)
Himalayan
Indosinian
Caledonian
Yangtze Craton
Cathaysia
Songpan Garze
Jianchuan Basin
U. Eocene
JN18 - Shuanghe
JN19 - Shuanghe
Shuanghe
Shuanghe-18
Jian-11-06 - Shuanghe
Lim-12-42 - Jinsichang
Jinsichang
Lim-12-26 - Baoxiangsi
Baoxiangsi
JN4 - Baoxiangsi
JN5 - Baoxiangsi
JN10 - Baoxiangsi
n=103
n=124
n=95
n=144
n=97
n=81
n=97
n=85
n=105
n=110
n=124
n=127
Yuanjiang Basin
U. Oligogene -Miocene
MY1
MY2
MY3
MY4
n=102
n=95
n=99
n=95
Simao Basin
U. Eoc-Oligoc.
Paleo-Eocene
XJG2400
XJG1670
XJG1210
XJG1075
XJG400
XJG20
n=104
n=92
n=98
n=83
n=97
n=92
Vietnamese Paleogene
U. Eocene-L. Oligocene
Lang Son-330-1
Lang Son-330-2
Na Duong-330-4
Na Duong-330-5
Na Duong-2009
That Ke TK1
That Ke TK2
Cao Bang CB4
Cao Bang CB8
Cao Bang CB10
Cao Bang CB12
n=135
n=143
n=112
n=135
n=97
n=113
n=130
n=132
n=115
n=141
n=123
Vietnamese Neogene
U. Miocene, Song Lo
U. Miocene, Yen Bai
U. Miocene, Song Lo
n=94
n=87
n=65
Gulf of Tonkin
Qiongdongnan, Y211UO - Upper Oligocene
Qiongdongnan, Y211LO - Lower Oligocene
n=89
n=117
0
500
1000
1500
2000
2500
3000
Age [Ma]

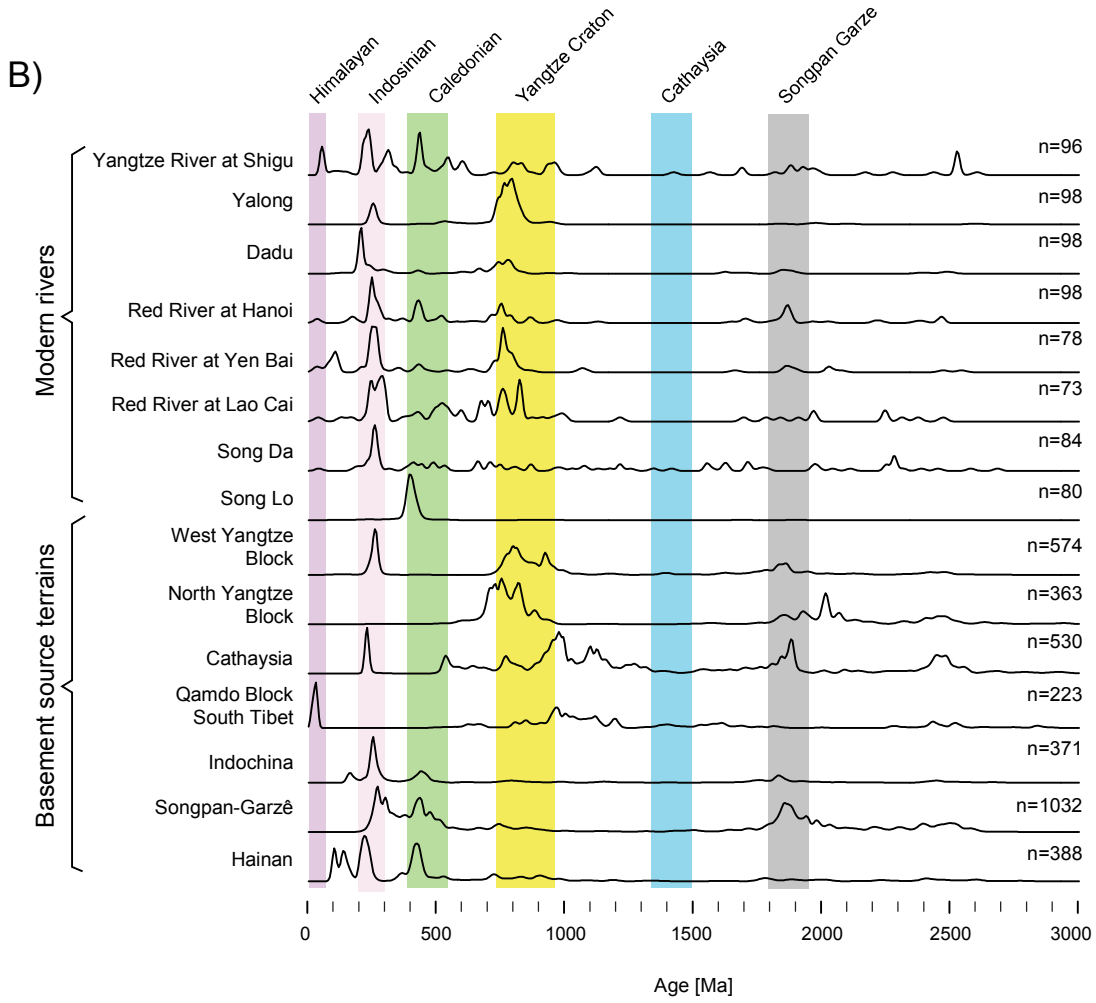
B)
Himalayan
Indosinian
Caledonian
Yangtze Craton
Cathaysia
Songpan Garze
Modern rivers
Basement source terrains
Yangtze River at Shigu
Yalong
Dadu
Red River at Hanoi
Red River at Yen Bai
Red River at Lao Cai
Song Da
Song Lo
West Yangtze Block
North Yangtze Block
Cathaysia
Qamdo Block South Tibet
Indochina
Songpan-Garzê
Hainan
n=96
n=98
n=98
n=98
n=78
n=73
n=84
n=80
n=574
n=363
n=530
n=223
n=371
n=1032
n=388
0
500
1000
1500
2000
2500
3000
Age [Ma]

Figure 9.

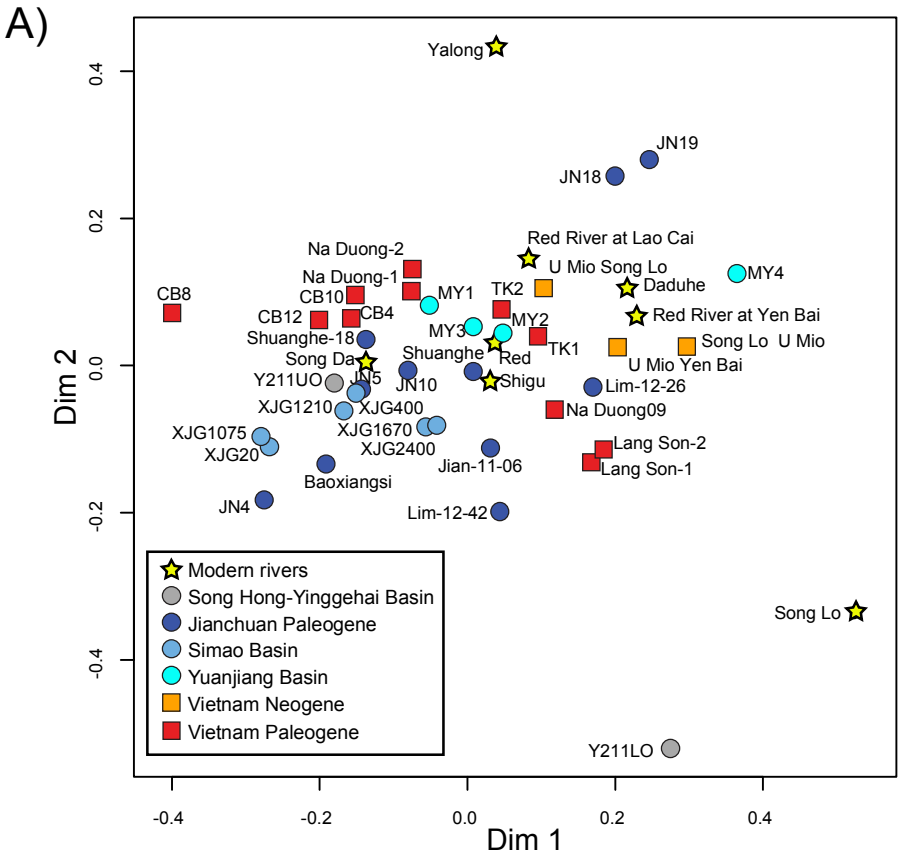
A)
Yalong
JN19
JN18
Red River at Lao Cai
Na Duong-2
U Mio Song Lo
Na Duong-1
MY4
Daduhe
CB8
CB10
MY1
TK2
CB12
CB4
MY2
Red River at Yen Bai
MY3
Shuanghe-18
TK1
Song Lo U Mio
Song Da
Shuanghe
Red
U Mio Yen Bai
Y211UO
JN5
JN10
Shigu
Lim-12-26
XJG1210
XJG400
Na Duong09
XJG1075
XJG1670
Lang Son-2
XJG20
XJG2400
Jian-11-06
Lang Son-1
Baoxiangsi
JN4
Lim-12-42
Modern rivers
Song Hong-Yinggehai Basin
Jianchuan Paleogene
Simao Basin
Yuanjiang Basin
Vietnam Neogene
Vietnam Paleogene
Song Lo
Y211LO
Dim 2
Dim 1
0.4
0.2
0.0
-0.2
-0.4

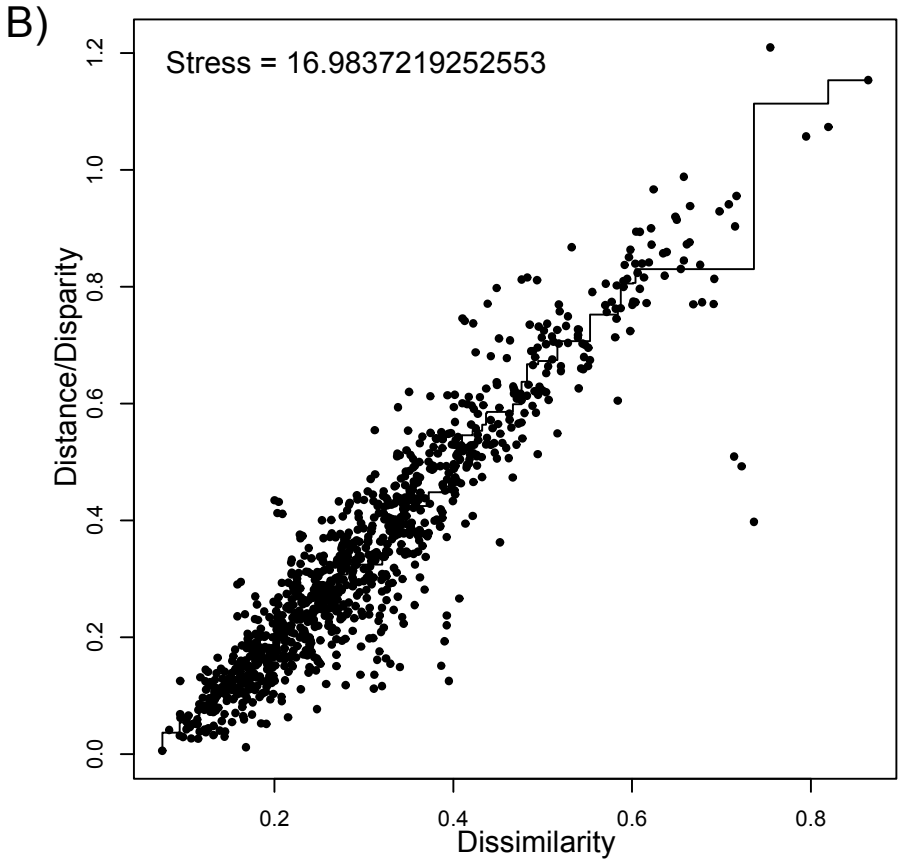
B)
Stress = 16.9837219252553
Distance/Disparity
Dissimilarity
0.0
0.2
0.4
0.6
0.8
1.0
1.2

Figure 10.

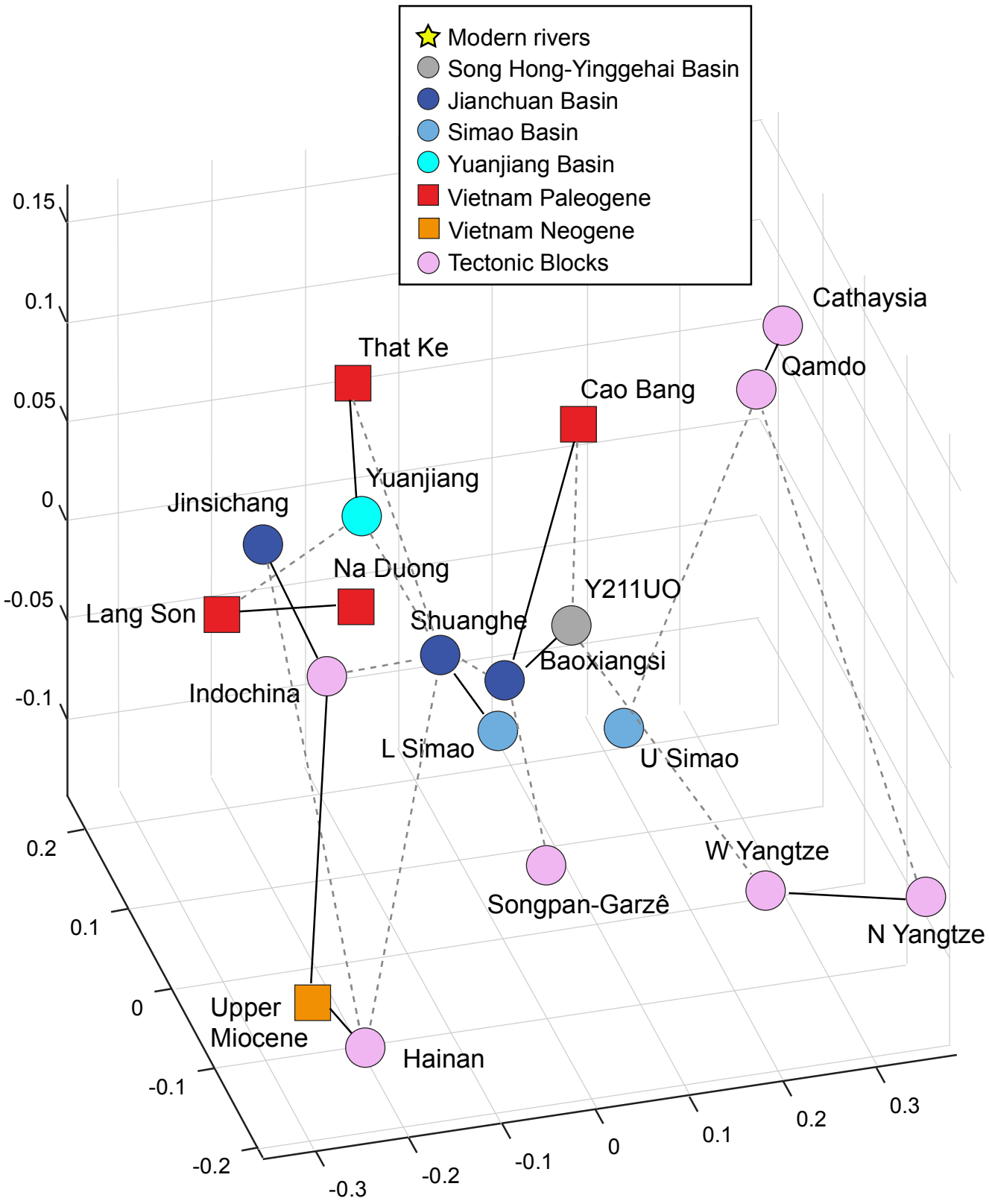
Modern rivers
Song Hong-Yinggehai Basin
Jianchuan Basin
Simao Basin
Yuanjiang Basin
Vietnam Paleogene
Vietnam Neogene
Tectonic Blocks
Cathaysia
Qamdo
That Ke
Cao Bang
Yuanjiang
Jinsichang
Na Duong
Lang Son
Y211UO
Shuanghe
Baoxiangsi
Indochina
L Simao
U Simao
W Yangtze
Songpan-Garzê
N Yangtze
Upper
Miocene
Hainan
0.15
0.1
0.05
0
-0.05
-0.1
0.2
0.1
0
-0.1
-0.2
-0.3
-0.2
-0.1
0
0.1
0.2
0.3

Figure 11.

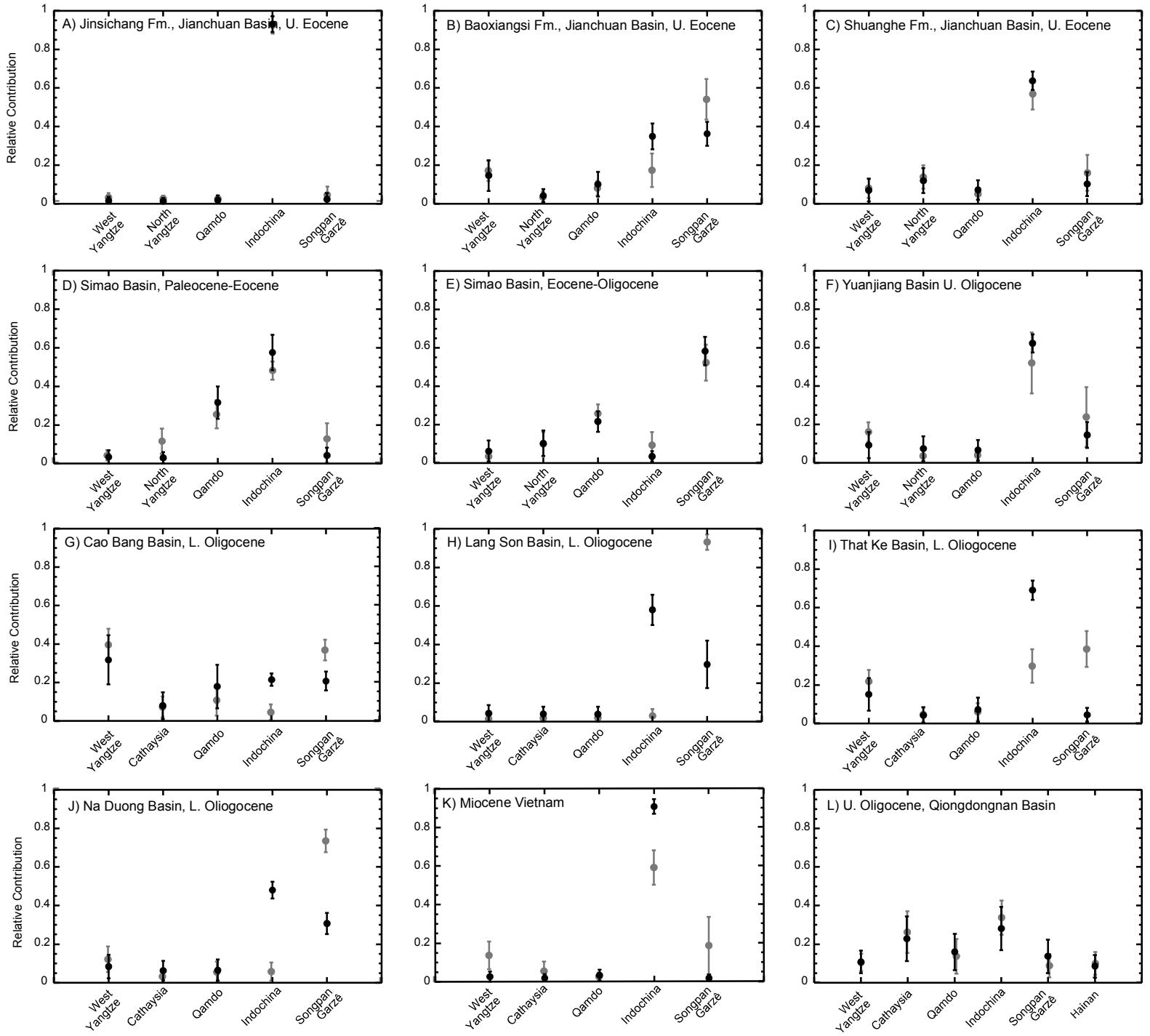
A) Jinsichang Fm., Jianchuan Basin, U. Eocene
B) Baoxiangsi Fm., Jianchuan Basin, U. Eocene
C) Shuanghe Fm., Jianchuan Basin, U. Eocene
D) Simao Basin, Paleocene-Eocene
E) Simao Basin, Eocene-Oligocene
F) Yuanjiang Basin U. Oligocene
G) Cao Bang Basin, L. Oligocene
H) Lang Son Basin, L. Oliogocene
I) That Ke Basin, L. Oliogocene
J) Na Duong Basin, L. Oliogocene
K) Miocene Vietnam
L) U. Oligocene, Qiongdongnan Basin
Relative Contribution
0
0.2
0.4
0.6
0.8
1
West Yangtze
North Yangtze
Cathaysia
Qamdo
Indochina
Songpan Garzê
Hainan

Figure 12.

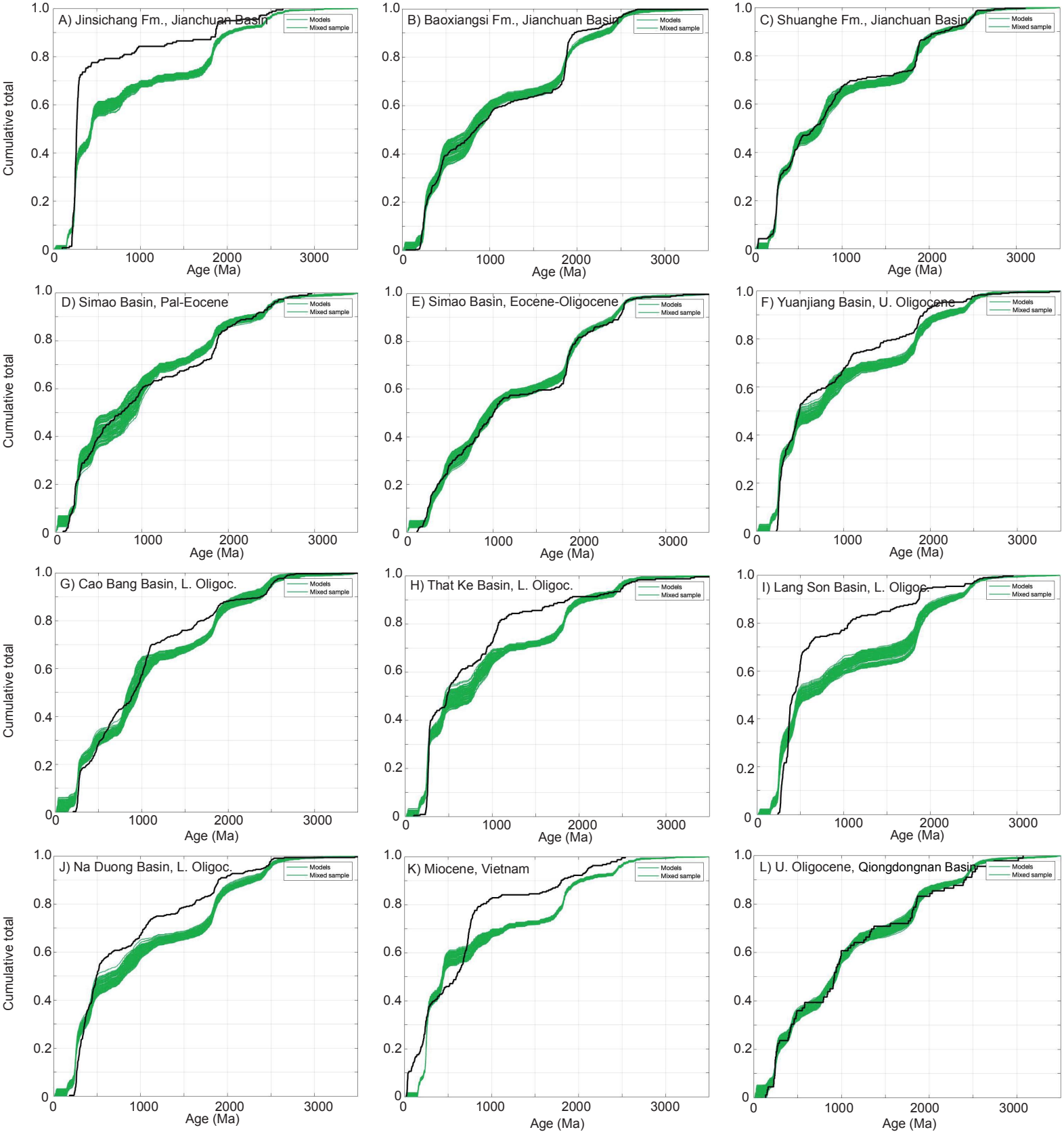
A) Jinsichang Fm., Jianchuan Basin
B) Baoxiangsi Fm., Jianchuan Basin
C) Shuanghe Fm., Jianchuan Basin
D) Simao Basin, Pal-Eocene
E) Simao Basin, Eocene-Oligocene
F) Yuanjiang Basin, U. Oligocene
G) Cao Bang Basin, L. Oligoc.
H) That Ke Basin, L. Oligoc.
I) Lang Son Basin, L. Oligoc.
J) Na Duong Basin, L. Oligoc.
K) Miocene, Vietnam
L) U. Oligocene, Qiongdongnan Basin
Models
Mixed sample
Cumulative total
Age (Ma)
0
0.2
0.4
0.6
0.8
1.0
1000
2000
3000

Figure 13.

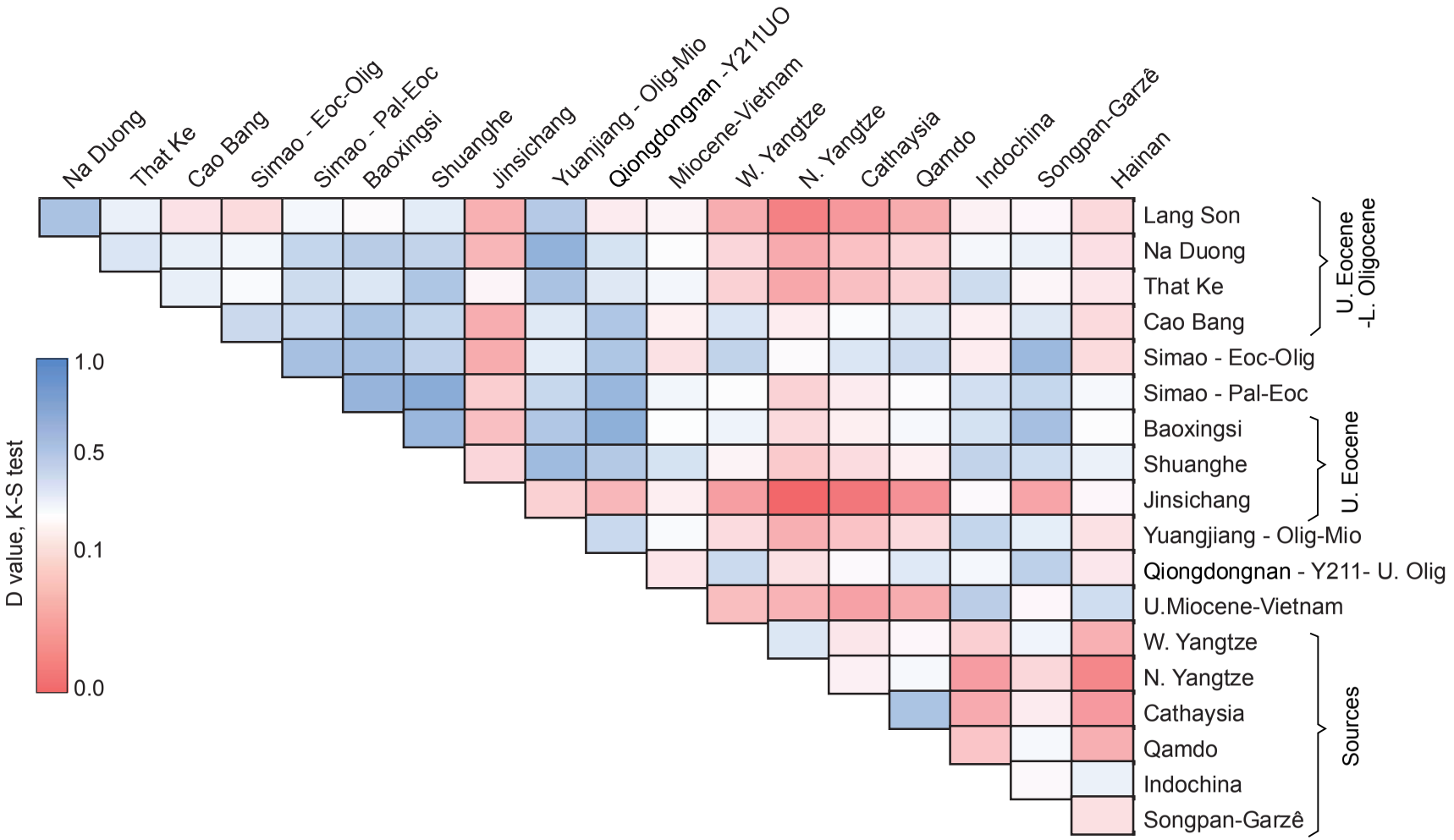

Figure 13
Clift et al.

Figure 14.

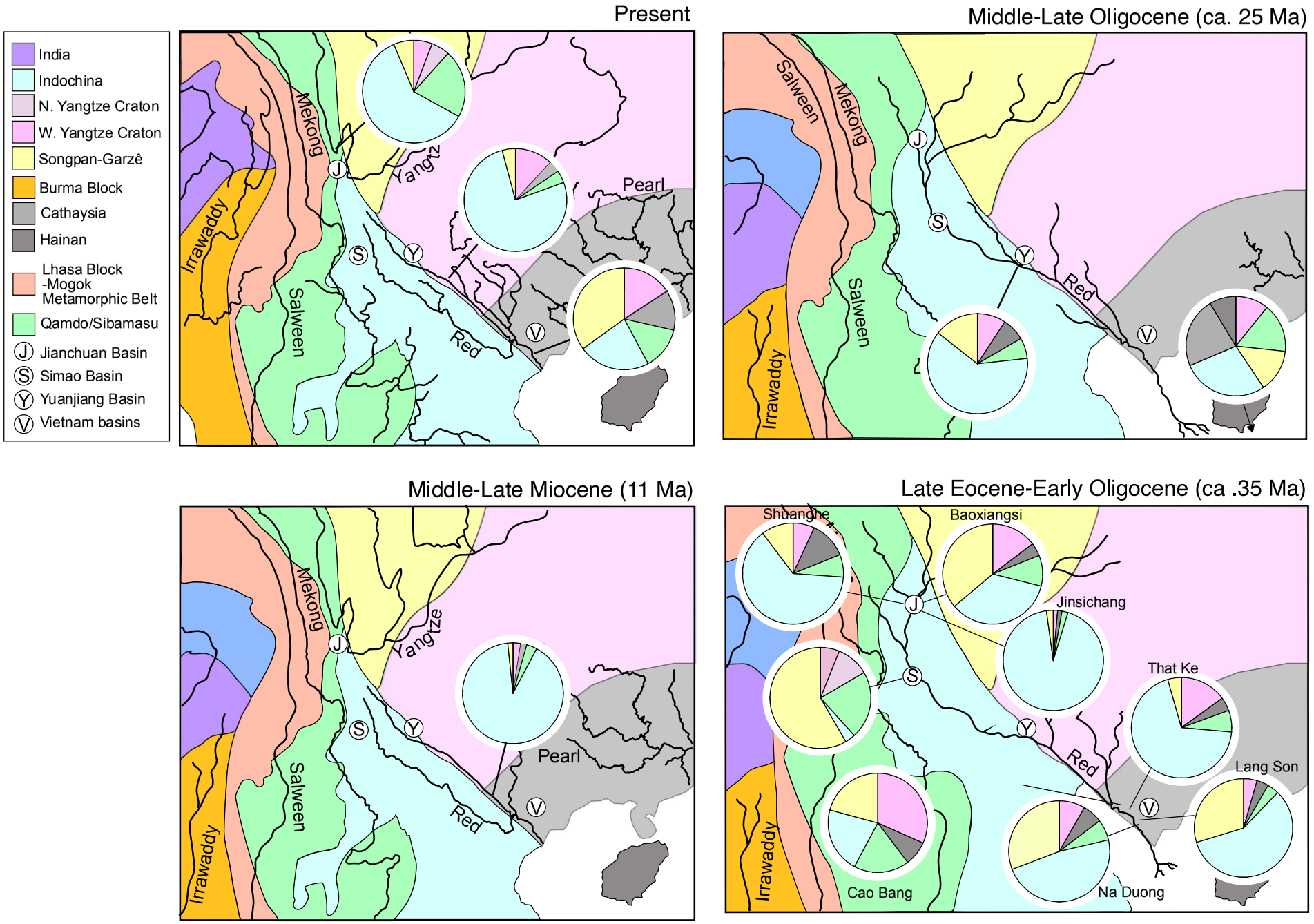
India
Indochina
N. Yangtze Craton
W. Yangtze Craton
Songpan-Garzê
Burma Block
Cathaysia
Hainan
Lhasa Block -Mogok Metamorphic Belt
Qamdo/Sibamasu
Jianchuan Basin
Simao Basin
Yuanjiang Basin
Vietnam basins
Present
Mekong
Yangtze
Pearl
Irrawaddy
Salween
Red
Middle-Late Oligocene (ca. 25 Ma)
Salween
Mekong
Red
Irrawaddy
Middle-Late Miocene (11 Ma)
Mekong
Yangtze
Pearl
Salween
Red
Irrawaddy
Late Eocene-Early Oligocene (ca .35 Ma)
Shuanghe
Baoxiangsi
Jinsichang
That Ke
Lang Son
Red
Irrawaddy
Cao Bang
Na Duong